0 0 0 0 4 7 0 3 6 2 6

LBL-5911
UC-59
TID-4500-R65

RECEIVED
LAWRENCE
BERKELEY LABORATORY

APR 22 1977

LIBRARY AND
DOCUMENTS SECTION

For Reference

Not to be taken from this room

Energy and Environment Division

Performance of an Experimental Solar-Driven Absorption Air Conditioner--Annual Report July 1975-Sept. 1976

Kim Dao, Melvin Simmons, Richard Wolgast and Michael Wahlig

January 1977

Lawrence Berkeley Laboratory University of California/Berkeley

Prepared for the U.S. Energy Research and Development Administration under Contract No. W-7405-ENG-48

LBL-5911 c.1

LEGAL NOTICE

This report was prepared as an account of work sponsored by the United States Government. Neither the United States nor the United States Energy Research and Development Administration, nor any of their employees, nor any of their contractors, subcontractors, or their employees, makes any warranty, express or implied, or assumes any legal liability or responsibility for the accuracy, completeness or usefulness of any information, apparatus, product or process disclosed, or represents that its use would not infringe privately owned rights.

Printed in the United States of America
Available from
National Technical Information Service
U.S. Department of Commerce
5285 Port Royal Road
Springfield, Virginia 22161
Price: Printed Copy $5.50; Microfiche $2.25

0 0 0 0 4 7 0 5 6 2 7

LBL-5911

PERFORMANCE OF AN EXPERIMENTAL SOLAR-DRIVEN ABSORPTION AIR CONDITIONER

Kim Dao
Melvin Simmons
Richard Wolgast
Michael Wahlig

Lawrence Berkeley Laboratory
University of California
Berkeley, California 94720

January 1977

ANNUAL REPORT

Covering the period July 1975 through September 1976

0 0 0 0 4 7 0 0 0 2 8

TABLE OF CONTENTS

SUMMARY 1

1. INTRODUCTION 2

2. DESCRIPTION OF THE EXPERIMENTAL UNIT 4

3. EXPERIMENTAL RESULTS 6

3.1. Experimental Procedure 8

3.2. Evaluation of the Equilibrium States at the Inlets and Outlets of the Components 13

3.3. Stability of Operation 14

3.4. Pressure Drop Across the Absorber 15

3.4.1. Basis for calculation of ΔP across the coils . . . 16

3.4.2. ΔP for the parallel coils after reconnection . . . 20

3.4.3. Influence of ΔP on system performance 22

3.5. Overall Heat Transfer Coefficient U for the Generator 23

3.5.1. Method of calculation of U from experimental data . 23

3.5.2. A correlation for h_{SS} based on forced convection . 25

4. DISCUSSION OF THE PERFORMANCE OF THE SYSTEM 28

4.1. Estimation of the Theoretical Maximum Coefficient of Performance 28

4.2. Practical Coefficient of Performance 36

4.2.1. Influence of the precooler 36

4.2.2. Influence of the preheater 36

4.3.3. Influence of the rectifier 37

4.3.4. Influence of the analyzer 38

4.2.5. Influence of the strong solution recirculation coil in the absorber 38

4.2.6. Calculation of practical COP 40

4.3. Possible Range of Operation 41

5. CONCLUSION 50

REFERENCES 51

APPENDIX I: Component Specifications 52

APPENDIX II: Experimental Data (Tables 1-10) 55

0 0 0 0 4 7 0 0 5 2 9

SUMMARY

An important pathway for the use of solar energy for space conditioning of buildings is the development of a heat-actuated air conditioner that can operate with the temperatures available from flat-plate solar collectors and use air cooling for disposal of the waste heat. The solar heating and cooling program of the Lawrence Berkeley Laboratory is exploring the use of the ammonia-water absorption cycle for this purpose. This report presents results of the initial tests of an experimental system that has been fabricated to provide basic engineering data on the operation of the ammonia-water absorption cycle under such conditions.

A nominal three-ton, continuous operation, heat-actuated water chiller has been fabricated by drastic modification of a commercial gas-fired unit. The major modifications included designing a new water-heated generator, adding a preheater to the solution circuit, and increasing the flow rate of solution by a factor of about three. The unit was instrumented for measurement of temperatures, pressures, and solution concentrations at points in the circuit. Twenty-two experimental runs have been made and the results analyzed.

Operation of the unit was found to be very stable, even at conditions near the thermodynamic cut-off point. There appear to be no localized non-equilibrium states whose interactions could cause instabilities. The unit operated dependably with a coefficient of performance (COP) of 0.6 to 0.7. Initial tests revealed a high pressure drop across the absorber that had an adverse effect on the temperature reached by the evaporator. Reconnecting the absorber into parallel sections significantly reduced the pressure drop, though not to the level ultimately desired. The method of Martinelli is shown to explain correctly the pressure drop across the absorber.

Analysis of the heat transfer to the solution in the generator shows that the desired condition of enhanced surface pool boiling was not achieved. An analysis based on the dominance of forced convection heat transfer is shown to explain the experimental data.

An analysis of the thermodynamic cycle which includes the finite effectiveness of heat transfer at various points in the cycle is shown to predict with good accuracy the measured values of COP. The measured coefficient of performance agreed with the calculated values over the range 0.4 to 0.75 as the conditions of individual runs were varied. The agreement with the calculated values was within about 5%.

The analysis used successfully to interpret the experimental data is then used to predict the possible range of operation of the ammonia-water absorption cycle. This range is shown to be compatible with the goal of operation with flat-plate solar collectors and air cooling; namely, the achievement of a COP $\gtrsim$ 0.6 using solar-heated hot water of 210°F or less, and an outdoor air temperature of 95°F for removing heat from the condenser and absorber coils.

1. INTRODUCTION

One of the important pathways to economical use of solar energy in buildings is the development of an air conditioner which can be driven by the low temperature heat ($\lesssim$ 210°F) obtained from flat-plate solar collectors. Absorption refrigeration systems have been demonstrated to be compatible with solar operation and probably constitute today's leading technology for solar cooling of buildings. Many combinations of refrigerant-absorbent pairs have been studied and evaluated (in absorption units driven by fossil fuels), but only the pairs NH_3-H_2O and H_2O-LiBr have been widely used.

A principal disadvantage of the H_2O-LiBr system is the danger of crystallization of the LiBr solution, which occurs if the temperature of the absorber is too high relative to the generator temperature. Air-cooled condensers and absorbers are limited by economic constraints (i.e., reasonable size) to condensing temperatures of 105°F and above, assuming a cooling air dry-bulb temperature of 95°F. Thus, operation of H_2O-LiBr systems from flat-plate solar collectors almost certainly requires evaporative cooling towers, thereby introducing high maintenance costs and appreciable consumption of water.

The NH_3-H_2O system has no hazard of crystallization; however, a serious disadvantage of the NH_3-H_2O system is the toxicity of the refrigerant NH_3. In order to guarantee that no ammonia enters the living area, some sort of liquid (usually a mixture of water and anti-freeze) must be used to transfer the heat from the conditioned space to the evaporator. This additional heat exchange loop increases the cost of the NH_3-H_2O system and also decreases the coefficient of performance (COP), since the evaporating temperature must be reduced to compensate for the temperature difference between the evaporator and this intermediate loop.

On the judgment[1] that elimination of the cooling tower for water-cooling the condenser was an overriding concern in development of a practical solar cooling system for residential applications, it was decided to pursue the development of the NH_3-H_2O system for such applications. Ammonia-water absorption units, with air-cooling of the condenser and absorber coils, have been produced commercially, but these gas-fired units operate at generator temperatures of approximately 350°F. The objective of this project, then, has been the extension of this technology to operate at lower generator temperatures ($\lesssim$ 210°F), while maintaining a viable COP ($\gtrsim$ 0.6). The final design of this chiller must lead to a unit that can be manufactured and sold at a competitive price in the marketplace.

2. DESCRIPTION OF THE EXPERIMENTAL UNIT

It was decided to obtain a gas-fired, air-cooled, ammonia-water absorption chiller as a starting point for the fabrication of an initial experimental solar-driven unit. The unit obtained was an ARKLA model ACB-60 which had a rated capacity of 5 tons when gas-fired.[1] The modification of this gas-fired unit was based on the following considerations:

i. The hot gas-to-liquid type generator of the gas-fired unit had to be replaced by liquid-to-liquid type generator for the solar unit. The new generator also had to be larger (i.e., more heat transfer surface area), because the liquid-to-liquid temperature difference for the solar unit would only be approximately 10°F, instead of hundreds of degrees fahrenheit for the gas-fired unit. It was decided to use a packed-tower counterflow heat exchanger for the generator.

ii. The circulation ratio (pounds of weak solution per pound of refrigerant) was about 2 for the gas-fired unit but had to be about 10 or more for the solar unit. Thus the solution pump had to be larger for the solar unit. For an anticipated capacity of 3 tons, two more solution pumps were added in parallel with the original solution pump.

iii. Since the circulation ratio would be greater, the need to recover the heat from the solution was more critical for the solar unit than for the gas-fired unit. Thus a preheater (weak solution to strong solution heat exchanger) was added.

iv. The concentration of water in the vapor from the generator was about 20% for the gas-fired unit and only about 2% for the solar unit. Thus the need to rectify the vapor was more critical for the gas-fired unit than for the solar unit, and only a small rectifier (with a by-pass) was incorporated in the solar unit.

v. To reduce the pressure drop across the absorber, the air-cooled absorber coils were reconnected to make three parallel coils, instead of the original configuration of a long coil in series with three short parallel coils. The reconnection was made after a few preliminary runs that indicated the total pressure drop in the original configuration reached 15 psi for an absorbent flow rate of 400 lbs/hr (about 1 gallon per minute).

Figure 1 shows the configuration of the experimental solar unit. Construction details of the generator and physical data for the components of the solar unit can be found in Appendix I.

3. EXPERIMENTAL RESULTS[2]

The experimental testing program had several principal objectives:

i. To test the agreement between the experimental data and the cycle calculations. The latter were based on assumed equilibrium states of the solutions and vapors at the inlets and outlets of the components of the system. (Equilibrium thermodynamic properties of the ammonia-water solution were taken from Research Bulletin No. 34, "Physical and Thermodynamic Properties of Ammonia-Water Mixtures", published by the Institute of Gas Technology, AGA, 1964).

ii. To determine the stability of operation near the cut-off conditions (very small differences in concentrations between the strong and weak solutions) of low generator temperatures and high condenser and absorber temperatures.

iii. To determine the effect of the pressure drop across the absorber on the COP and the evaporator temperature.

iv. To determine the overall performance of the generator and compare to the design goals.

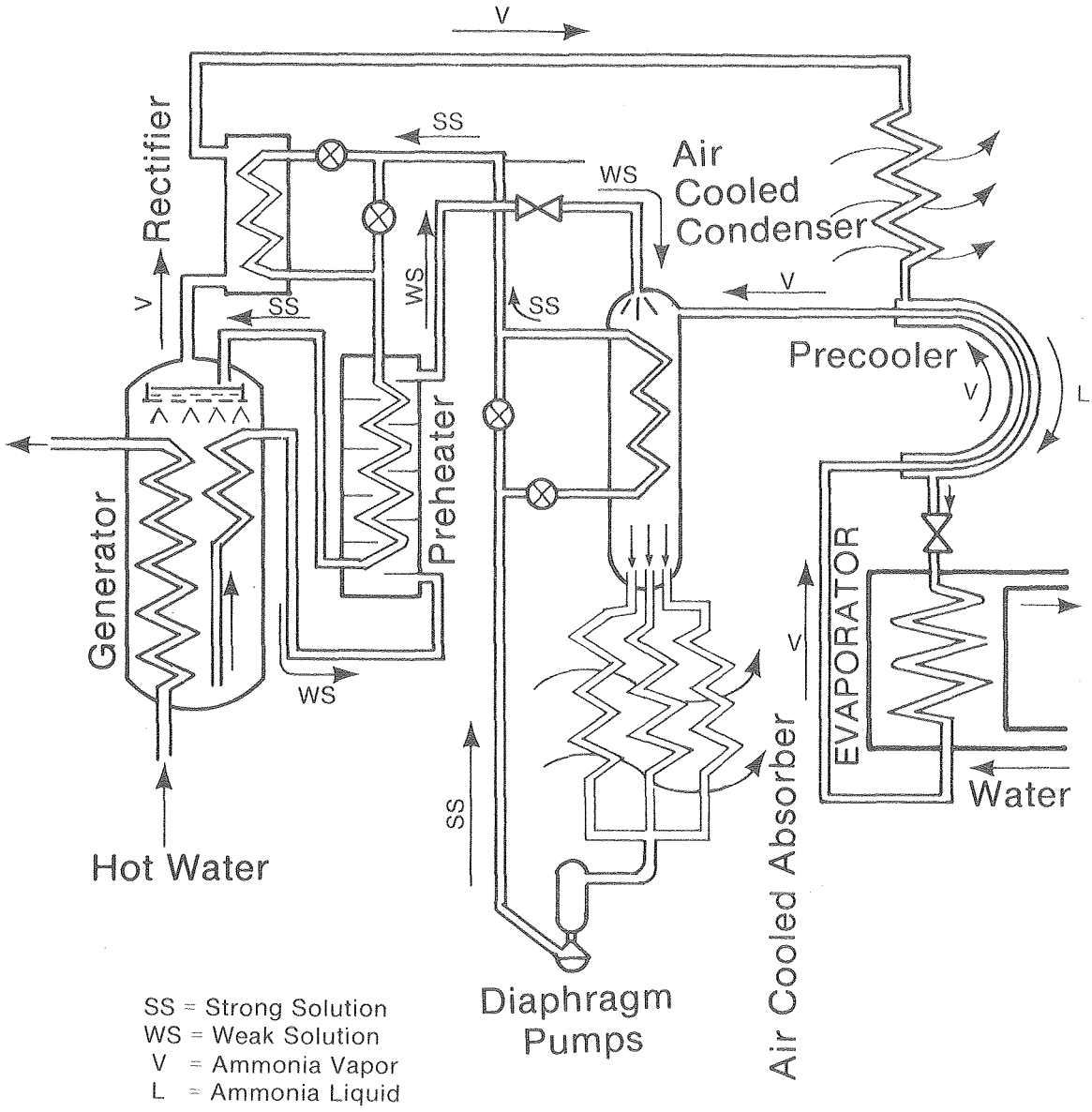

XBL 771-140

Fig. 1. Schematic diagram of the absorption air conditioner as modified for solar operation.

3.1 Experimental Procedure

Figure 2 shows the measurement locations designed into the experimental unit. Temperature measurements were made with copper-constantan thermocouple wires (20 gauge), silver-soldered to the external surface of the tubing and covered with thermal insulation. A digital voltmeter was used for direct reading of the temperature, and was calibrated to an accuracy of ± 0.1°C at the ice point and ± 0.2°C at the boiling point of water.

Pressures were measured with Bourdon gauges calibrated to ± 1 psi (compound, 6" dial Marshall Town-Permagage at 150 psi for low pressures and 300 psi for high pressures).

The mass flow rates of the ammonia and of the weak solution were measured with Safeguard Rotameters calibrated to ± 2% accuracy.

The concentrations of the weak and strong solutions were measured with small sampling chambers built into the solution circuits. Each sampling chamber consisted of a tube in parallel with the solution line. Valves installed at each end of the tube could isolate it from the solution flow. A stainless steel adjustable bellows connected to the tube could increase or decrease the volume by ± 2%. To make a measurement, the valves were first opened to allow the solution to flow through the sampling tube, and then were closed. The bellows was then opened until the solution inside the tube was in equilibrium with a very small amount of vapor. The concentration was then determined by measuring the saturated pressure and temperature and by using the equilibrium data tables.

The flow rate of the hot water was measured using a mercury column installed across the generator hot water coils. The pressure drop indicated by the mercury column was previously calibrated against volumetric flow rates. The flow rate of the chilled water was measured by a mercury column

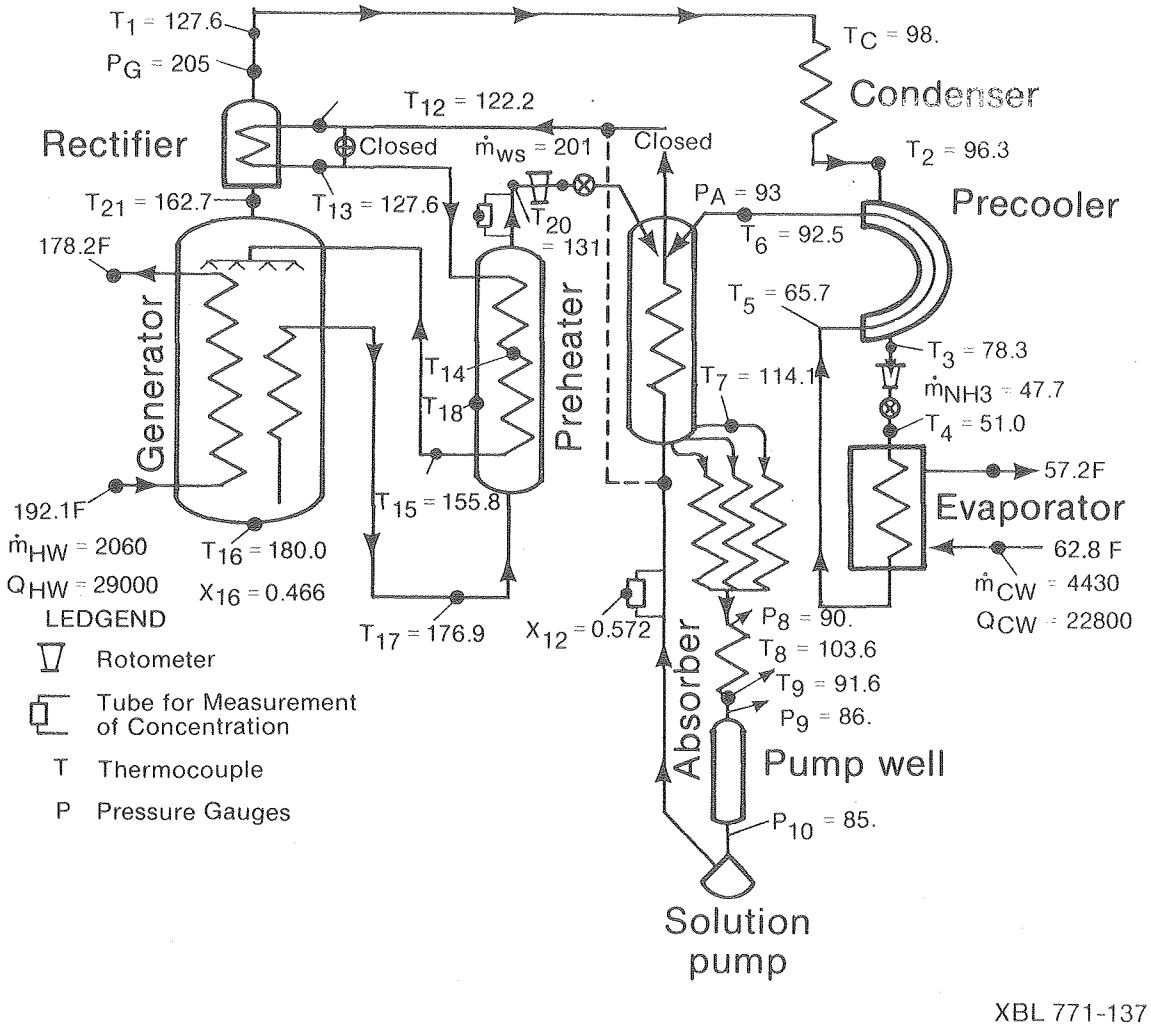

Fig. 2. Measurement locations with experimental data for Run 10C.

installed across a flow measuring valve. All water flow rates were calibrated to within ± 2% accuracy. The heat inputs to the generator (q_G) and evaporator (q_E) were calculated from the water flow rates and temperature drops. The specific heat of the hot water was taken to be 1.0 Btu/lb°F, and the specific heat of the chilled water (with antifreeze added) was taken to be 0.90 ± 0.01. Other sources of error in determining q_G and q_E were the inaccuracies of the measurement of the temperature drop, ΔT, across the water coils. ΔT was of the order of 5 ± 0.1°C, for a relative error of ± 2%. Total errors were ± 4% for q_G and ± 5% for q_E.

The system was charged with 65 lbs of solution of 55% ammonia concentration. The unit was then started by pumping hot water, controlled at constant inlet temperature, through the generator. The condenser-absorber fan and the solution pumps were turned on when the generator pressure reached about 150 psig. It took about 15 minutes to warm up the system to approximate steady-state running conditions.

The flow rates of ammonia and of the weak solution were then readjusted to desired values using expansion valves. Experimental data were taken 30 to 45 minutes after setting the running conditions in order to allow the system to reach steady-state.

Figures 2, 3, and 4 show the experimental data of three typical runs (runs 10C, 19B, and 20C).

The following symbols are used in Figures 2, 3, and 4:

$\dot{m}_{NH_3}$ = mass flow rate of ammonia, lbs/hr

$\dot{m}_{WS}$ = mass flow rate of weak solution, lbs/hr

$\dot{m}_{HW}$ = mass flow rate of hot water, lbs/hr

$\dot{m}_{CW}$ = mass flow rate of chilled water, lbs/hr

Q_{HW} = heat input from hot water, Btu/hr

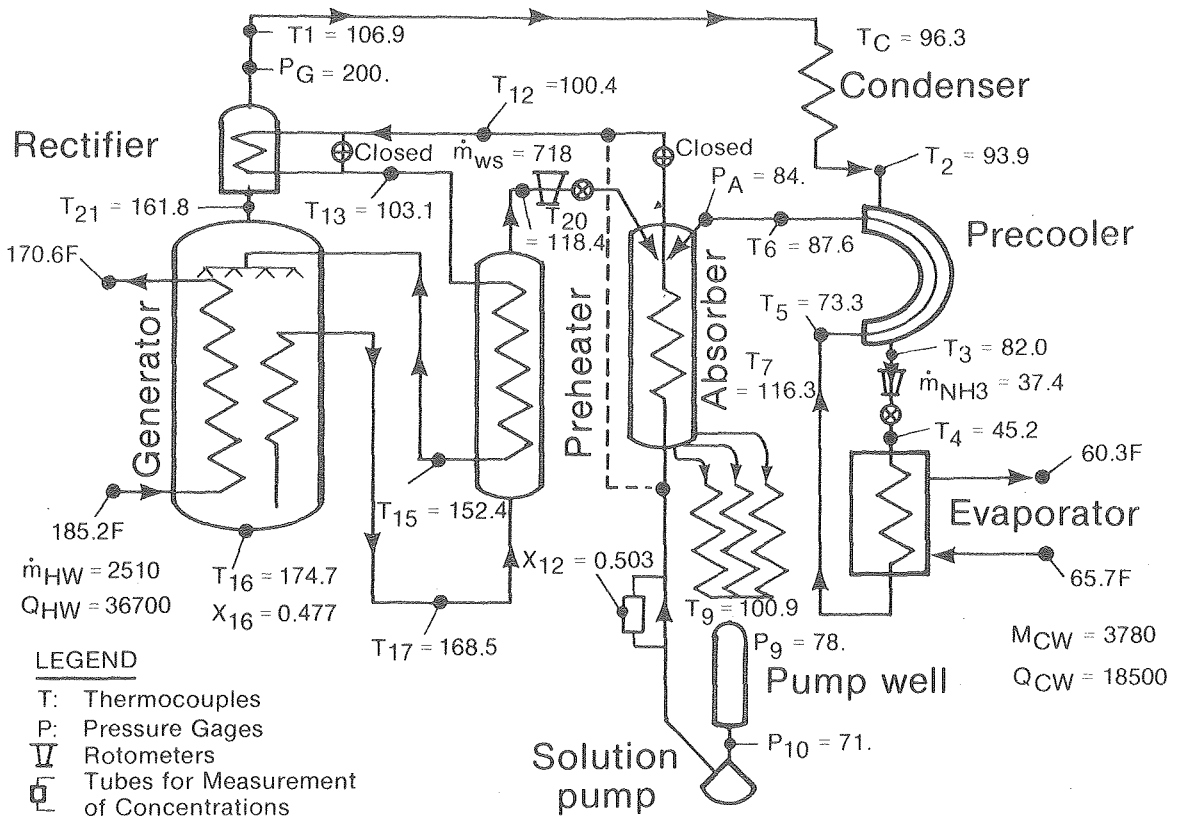

Fig. 3. Experimental data of Run 19B.

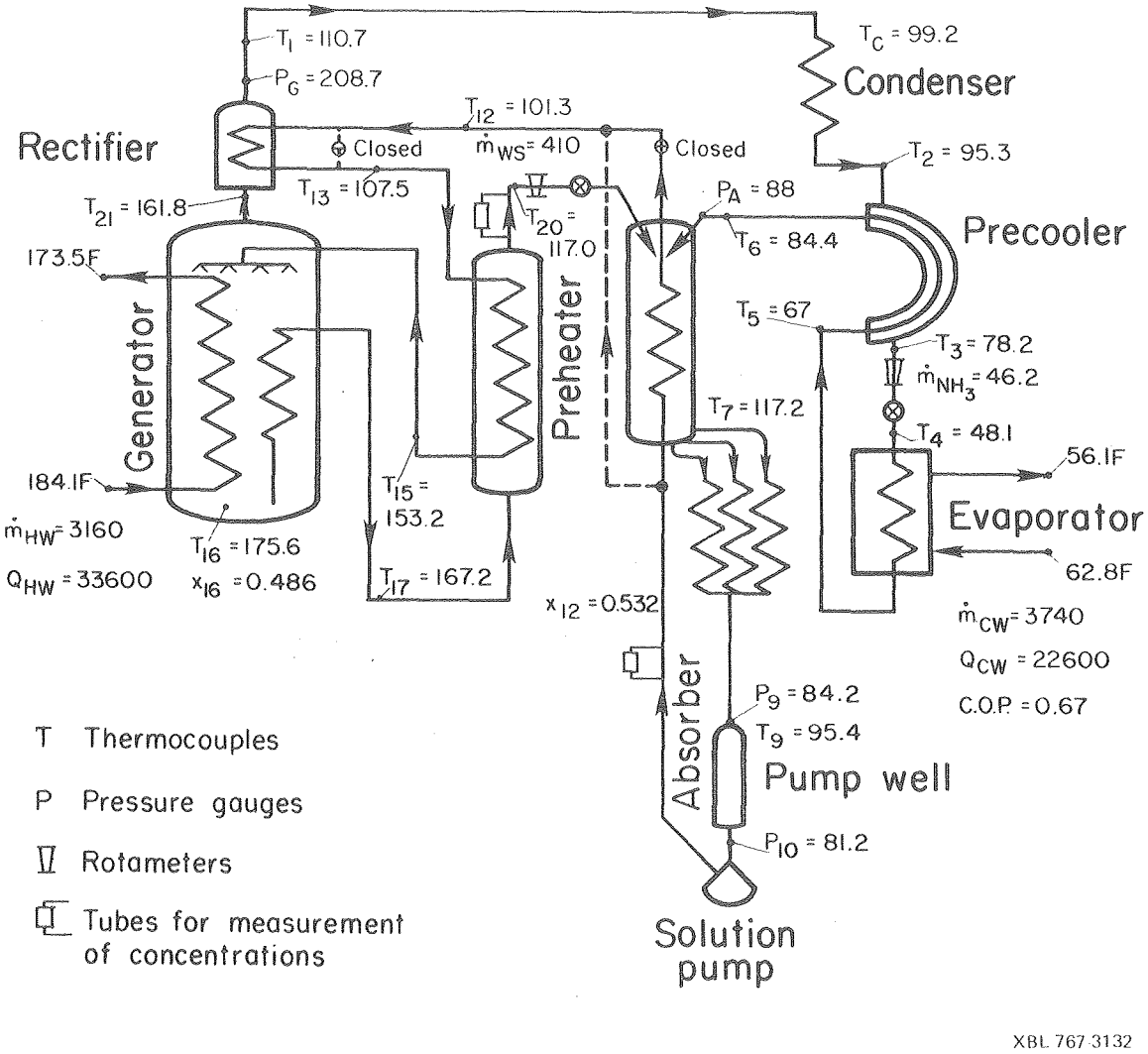

Fig. 4. Experimental data of Run 20C.

Q_{CW} = heat input from chilled water, Btu/hr

P = pressure, psia

T = temperature, °F

x = concentration, lbs of NH_3/lb of solution

T_C = condensing temperature, defined to be the temperature at which the vapor pressure of pure ammonia equals the pressure at the generator

3.2 Evaluation of the Equilibrium States at the Inlets and Outlets of the Components

Analytical calculations of the absorption cycle are possible only when the thermodynamic states of the solutions and vapors at the inlets and outlets of the system's components are assumed to be equilibrium states. When equilibrium states are assumed, tables of thermodynamic properties of the working fluids can be used in conjunction with the energy equations, continuity equations, and flow friction equations to estimate the performance of the cycle. The second law must also be used to determine the correct direction of the processes.

All runs made during the testing stage were found to confirm analytical calculations based upon the assumption of equilibrium states. That is: given the measured mass flow rates and the measured pressures and temperatures, the energy equations around the components can be satisfied, within the experimental error (about ± 5% or less), by using the equilibrium enthalpies. The mass balances can be satisfied by using the equilibrium concentrations.

Some particulars worth mentioning are:

i. The pressure at the inlet to the absorber did not equal the equilibrium evaporating pressure corresponding to the temperature (T_4) measured after the ammonia expansion

valve. This was because the expansion valve was located about 6 feet above the evaporator. The difference in pressure represented the hydrostatic pressure of 6 feet of liquid ammonia.

ii. A cyclic discharge of ammonia-water solution from the evaporator/precooler caused temperature fluctuations observed at the precooler vapor outlet (location 6 in Figs. 2 - 4). The water was carried by the vapor (which was 99.5% ammonia, 0.5% water) from the generator through the condenser, where it condensed and accumulated in the lower loops of the evaporator/precooler coils. Discharges of liquid would occur when the water-ammonia solution had accumulated sufficiently to block the passage. These cyclic discharges showed negligible effect on the time-averaged performance of the system.

3.3 Stability of Operation

The system required about 30 minutes to reach steady state due to the large mass of the solution charge. The steady state was reached without oscillations, even when a sudden change in the flow rates was made. The operation was very stable; the system did not show appreciable changes after hours of operation. The stability of operation extended to very low concentration differences between the weak and strong solutions (or, equivalently, very high circulation ratios, on the order of 20 or more).

For a high mass flow rate of the weak solution, the preheater effectiveness was low and the temperature of the weak solution entering the absorber

was high, causing a flashing of the weak solution in the absorber. This flashing did not influence the stability of operation of the system. A large pressure drop across the absorber also caused no oscillatory perturbations.

This proved that the absorption and evaporation of the solution occurred fast enough to produce approximately equilibrium states everywhere in the system. There appear to be no localized nonequilibrium states whose interactions could cause instabilities.

3.4 Pressure Drop Across the Absorber

A high pressure drop across the absorber increases the temperature of the evaporator from what could otherwise be obtained. Thus an important question for the design of a solar-driven air conditioner is how to minimize this pressure drop. Because we are using the absorber provided in the gas-fired unit, we are far from an optimum design.

Figure 2 shows the experimental data of Run 10C, taken before the air-cooled coils of the absorber were reconnected. Even at rather low flow rates of the ammonia (47.7 lbs/hr) and of the weak solution (201 lbs/hr), the total pressure drop was quite high (8 psi as measured across the absorber coils in series with the valves to the solution pumps).

The ΔP across the valves and filter to the solution pumps were proportional to the square of the flow rate of the strong solution:

$$\frac{\Delta P_{valves}}{(\text{flow rate})^2} \simeq 2.0 \text{ psi/(gpm)}^2 \qquad (1)$$

The ΔP across the coils, due to two phase flow friction, is discussed below.

3.4.1. Basis for calculation of ΔP across the coils

According to Martinelli's[3] method of calculation of ΔP for two phase flows, assuming a linear distribution of vapor quality along the pipe, ΔP should be very close to a linear function of $(\dot{m}_{Li} \cdot \dot{m}_{Vi})^{0.9}$, where $\dot{m}_{Li}$ and $\dot{m}_{Vi}$ are the mass flow rates of the liquid and of the vapor, respectively, at the inlet. (The liquid and vapor flows are cocurrent, and the outlet flows are $\dot{m}_{Vo} = 0$ and $\dot{m}_{Lo} = \dot{m}_{Li} + \dot{m}_{Vi}$.) Thus:

$$\Delta P = K(\dot{m}_{Li} \cdot \dot{m}_{Vi})^{0.9} + \Delta P_{\ell.0} + \Delta P_{hydro} + \Delta P_{mom} \quad .$$

$\Delta P_{\ell.0}$ is the pressure drop that would occur if the liquid were flowing alone at a rate $\dot{m}_{Li}$ through the same circuit. ΔP_{hydro} is the hydrostatic pressure differential between the inlet and outlet. (Here ΔP_{hydro} = 2.5 feet of solution = 1 psi.) ΔP_{mom} is the momentum pressure due to the transfer of the higher momentum of the vapor to the liquid when the vapor is absorbed into the liquid. Here ΔP_{mom} is about 3% of ΔP and is therefore neglected.

The coefficient K depends on the properties of the liquid and vapor, on the tube diameter and length, and also on the tube fittings along the circuit. In the absorber coils there are a number of 90° bends, 180° bends, tees, reducers, and connecting tubings. The influence of the fittings is estimated to be substantial, and thus they must be included in the analysis.

Martinelli's method[3] of calculation of ΔP produces the following expression for K:

$$K = \frac{1.83}{2gD_H^{1.2}\ A_F^{1.8}} \ \frac{(\mu_L \mu_V)^{0.1}}{(\rho_L \rho_V)^{0.5}} \ Le \quad , \qquad (2)$$

where Le is the equivalent length of the circuit:

$$Le = Lo + \Sigma \ell e \quad . \tag{3}$$

Thus Le consists of the sum of Lo, the total length of straight tubing where the absorption of vapor occurs, and a sum of terms, ℓe, which represent the equivalent length of each fitting in the circuit. The equivalent length of a fitting for two phase flow is approximated by the following expression:

$$\ell e = \frac{c}{15} \left(\frac{\rho_L}{\rho_V}\right)^{0.5} \left(\frac{\mu_L}{\mu_V}\right)^{0.1} \left(\frac{L_f}{Lo}\right) \ell' e \quad ,$$

where

$\ell' e$ = equivalent length of the fitting where only the liquid is flowing at $\dot{m}_{Li}$;

c = coefficient depending on the fitting; for example, $c = 2.2$ for long radius bends;[4]

L_f = length of straight tubing from the inlet to the fitting under consideration;

D_H = hydraulic diameter = inside diameter of tube;

A_F = flow cross-section area;

μ, ρ = viscosity and density; and

g = unit of force/(unit of mass × length × time^{-2}) .

The limitations on the use of the above equations are

$$\left(\frac{\dot{m}_{Li}}{\dot{m}_{Vi}}\right)^{0.9} \left(\frac{\mu_L}{\mu_V}\right)^{0.1} \left(\frac{\rho_V}{\rho_L}\right)^{0.5} > 0.5 \quad ,$$

with the Reynolds number, Re, of the liquid flowing alone > 2000, and Re of the vapor flowing alone, at inlet, > 5000.

NOTE: The above relation is derived assuming $\dot{m}_V$ decreases linearly from its value at inlet to zero at outlet. An assumption of parabolic distribution would result in a value of K about 15% lower than the linear case.

The value of K calculated for the series coil with these assumptions is:

$$K = 1.92 \times 10^{-5} \text{ Le} \qquad [\text{psi}/(\text{lb/hr})^{1.8}]$$

where the following values have been used:

L_e = equivalent circuit length, ft

D_H = 0.527 inch = 0.0439 ft

A_F = $\pi(0.527)^2/4$ = 0.001515 ft^2

μ_L = 1.2 lbm/hr-ft

μ_V = 0.026 lbm/hr-ft

ρ_L = 50 lbs/ft^3

ρ_V = 0.244 lb/ft^3

In calculating the contributions to Le, we use the approximations:

$\ell'e$ = 20D = 0.88 ft for 90° long radius bends

= 40D = 1.76 ft for 180° bends,

and then Le is calculated with equation (3).

For the long series coil before reconnection, Lo = 74 feet, and the fittings consist of one 90° bend at the inlet plus nine 180° bends equally spaced along the coil. Thus our assumptions lead to the estimate Le = 101 feet and $K = 1.94 \times 10^{-3}$ $\text{psi}/(\text{lb/hr})^{1.8}$. Then the pressure drop across the series coil, ΔP_s, due to the two-phase-flow contribution, is

$$\Delta P_s = \Delta P - \Delta P_{hydro} - \Delta P_{\ell.0} = 1.94 \times 10^{-3} (m_{Li} \cdot m_{Vi})^{0.9} .$$

As shown in Fig. 5, the calculated line fits the experimental points very well. (See Appendix II for experimental data.) Therefore the above method of calculating ΔP has been verified experimentally.

NOTE: In Fig. 5, $\dot{m}_{Li}$ was taken to be $(\dot{m}_{WS} + \frac{1}{2}\dot{m}_{NH_3})$ and it was assumed that $\dot{m}_V$ decreases proportinally with respect to the temperature;

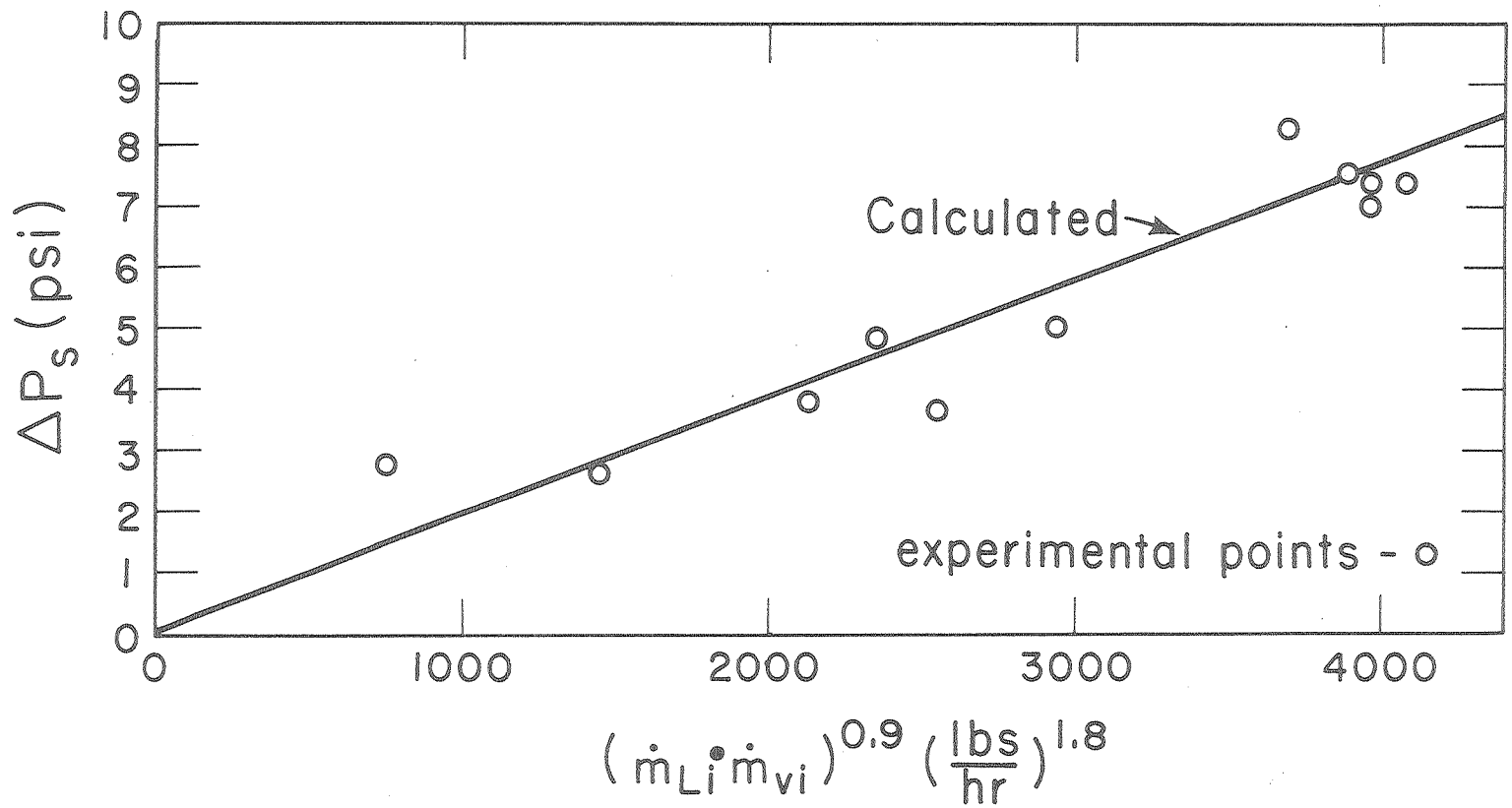

Fig. 5. Pressure drop across series coil before reconnecting the absorber. Experimental errors: on ΔP: ±2 psi max.; on $\dot{M}$: ±2% max.

XBL 771-142

that is:

$$\dot{m}_{Vi} = (\dot{m}_{NH_3} \text{ from evaporator}) \left(\frac{T_{\text{at inlet series coil}} - T_{out}}{T_{\text{at inlet absorber}} - T_{out}} \right),$$

where, referring to Fig, 2, $T_{\text{at inlet series coil}} = T_8$, $T_{\text{at inlet absorber}} = T_7$, and $T_{out} = T_9$. (See Appendix II for ratio $\dot{m}_{Vi}/\dot{m}_{NH_3}$ of the runs.)

3.4.2 ΔP for the parallel coils after reconnection

The sections of the absorber were reconnected to reduce pressure drop; however, in this modification the geometry of the three parallel coils is not identical and, since the number and nature of the fittings are different for the three coils, it is expected that the flow distribution will be uneven.

Let $\dot{m}_{LT}$ and $\dot{m}_{VT}$ be the total mass flow rates at the inlet of all three coils. Then the pressure drop, ΔP_p, across this configuration of the three coils in parallel is:

$$\Delta P_p = (\Delta P - \Delta P_{\ell.0} - \Delta P_{hydro}) = K_p (\dot{m}_{LT} \cdot \dot{m}_{VT})^{0.9} .$$

Experimental data after reconnection gives:

$$K_p = 0.426 \times 10^{-3} \text{ psi/(lbs/hr)}^{1.8} ,$$

as shown in Fig. 6.

Let $y_{1,2,3}$ be the fractions of the total mass flow rates through coils 1, 2, and 3. Then

$$\begin{aligned} \Delta P_{p1} &= 0.426 \times 10^{-3} (y_1)^{-1.8} (\dot{m}_{L1} \cdot \dot{m}_{V1})^{0.9} \\ &= 0.426 \times 10^{-3} (y_2)^{-1.8} (\dot{m}_{L2} \cdot \dot{m}_{V2})^{0.9} \\ &= \Delta P_p \end{aligned}$$

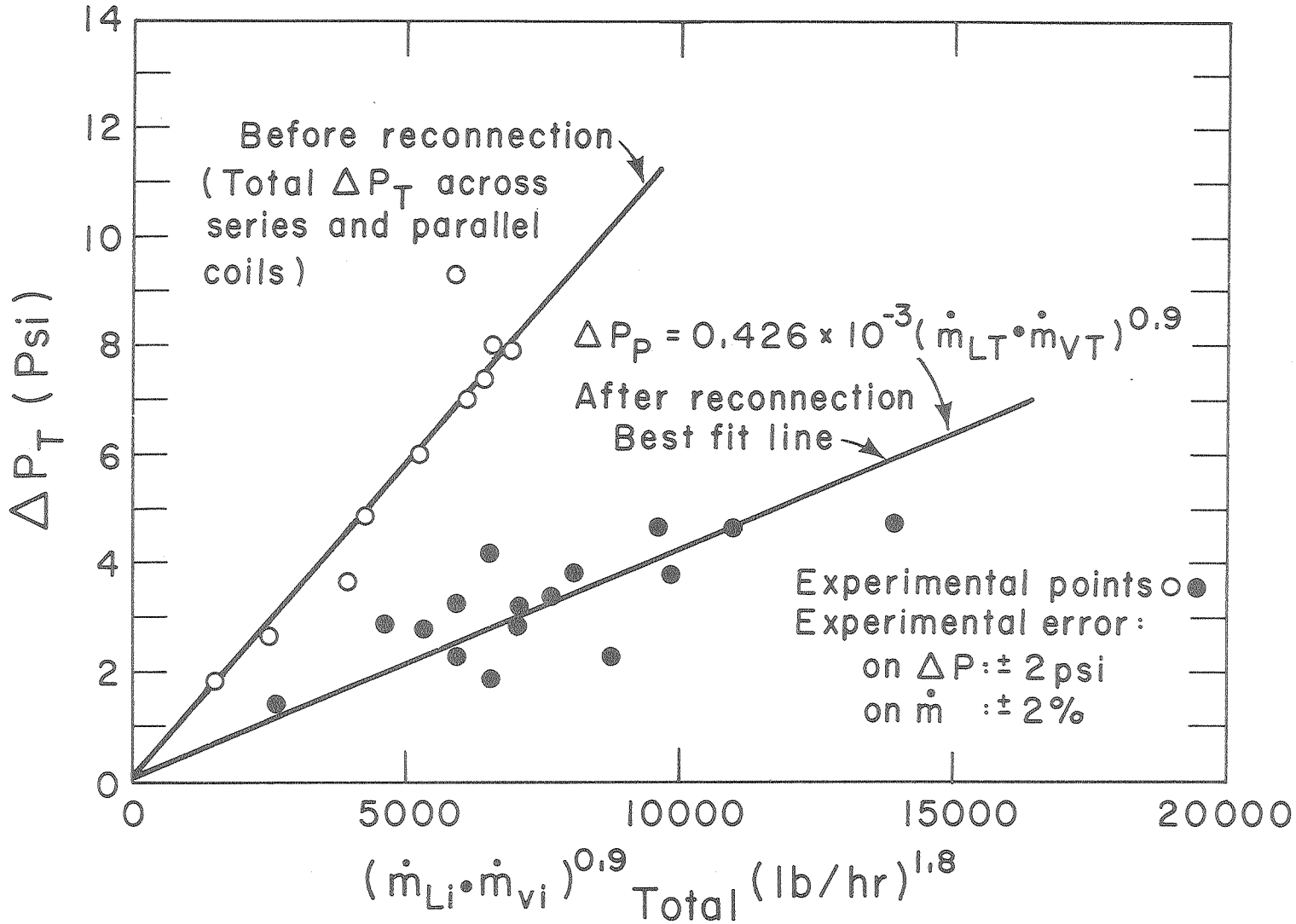

Fig. 6. ΔP_T across absorber due to two phase friction. This ΔP_T is simply the pressure drop ΔP_P across the parallel coils after reconnection, whereas before reconnection ΔP_T equals the pressure drop across both the series coil and the parallel coils.

XBL 771-147

with $y_1 + y_2 + y_3 = 1.0$, and $y_2 = y_3$ (coils 2 and 3 are identical). It is difficult to estimate the equivalent length of coils 2 and 3 because they involve non-standard fittings. The Le of coil 1 is 92 ft. Martinelli's method of calculation of ΔP_p yields $\Delta P_{p1} = 1.76 \times 10^{-3} (\dot{m}_{L1} \cdot \dot{m}_{V1})^{0.9}$. Therefore y_1 must be $[0.426 \times 10^{-3}/1.76 \times 10^{-3}]^{1/1.8} = 0.45$. So, $y_1 = 45\%$ and $y_2 = y_3 = 27.5\%$. This uneven distribution of flow rates increases ΔP substantially. Here the percentage increase is $(0.45/0.33)^{1.8} = 175\%$. Therefore a balanced flow distribution in all parallel coils is necessary.

3.4.3. Influence of ΔP on system performance

The net influence of the total pressure drop across the absorber is to increase the evaporating temperature T_E. The maximum concentration of the strong solution is determined by the temperature and the pressure at the solution pump wells, quite independently of the pressure at the evaporator. This pressure at the evaporator should be made equal to the pressure at the pump wells for the lowest possible T_E. A pressure drop of 8 psi across the absorber increases T_E by 5°F. For instance, $T_E = T_4$ of Run 10C (see Fig. 2) could be 47°F instead of 51°F, and $T_E = T_4$ of Run 19B (see Fig. 3) could be 39°F instead of 45.2°F if the absorber were better designed for solar operation.

This change in the evaporator temperature is the principal effect of the pressure drop ΔP from the evaporator to the pump well. ΔP may also affect the flashing of the weak solution entering the absorber, but this flashing does not significantly alter the final product of the absorption since the amount of heat removed from the absorber is not changed by the flashing, and the temperature of the solution at the inlet to the coils does not decrease appreciably. This flashing can be prevented by cooling

the weak solution sufficiently in a more efficient preheater.

3.5 Overall Heat Transfer Coefficient U for the Generator

3.5.1. Method of calculation of U from experimental data

In calculating the heat transfer coefficient of the generator, we treat U as an overall average value. We also assume that the strong solution, before contacting the hot water coils, is at its saturated temperature at the pressure P_G of the generator. This assumption is valid for most of the runs since the strong solution absorbs a small amount of vapor during its fall through the pall rings (see Appendix I) before contacting the hot water coils. This absorption of vapor rapidly raises the temperature of the strong solution to its saturation state, with an associated change in concentration.

Since most of the tube surface of the analyzer is upstream of the hot water coils, the influence of the analyzer (the weak solution recirculation coil) is to evaporate part of the ammonia content of the strong solution, thus changing further the saturation temperature T_{SS} of the strong solution before the latter can reach the hot water coils. The change in saturation temperature is estimated from the sensible heat capacities of the weak and strong solutions (approximately 1.14 Btu/lb-F) and from an equivalent heat capacity of the strong solution (approximately 5.4 Btu/lb-F) that includes the latent heat of evaporation. The change in saturation temperature of the strong solution is then given by:

$$\Delta T_{SS} = \frac{1.14}{5.4}\left[\frac{\dot{m}_{WS}}{\dot{m}_{SS}}(T_{16} - T_{17}) - (T'_{SS} - T_{15})\right] = T_{SS}^{(\text{reaching hot coil})} - T'_{SS} ,$$

where T'_{SS} can be taken as the saturation temperature at P_G and at the

concentration x_{15} before entering the generator.

The coefficient U is calculated from

$$U = \frac{Q_{Hot\ Water}}{36\ ft^2 \times \Delta T_m}$$

where

$$\Delta T_m = \frac{(T_{HW,in} - T_{16}) - (T_{HW,out} - T_{SS})}{\ln \frac{T_{HW,in} - T_{16}}{T_{HW,out} - T_{SS}}}$$

Typical values of U obtained during the experimental test runs were in the range 50 - 150 Btu/hr-ft^2-F.

The heat transfer coefficient on the water side is approximately (with twisted tape insert in tubes):

$$h_{HW} = 0.046 \times \frac{k}{D_H} (Re_H)^{0.8} (Pr)^{0.3} \simeq \left(\frac{\dot{m}_{HW}}{1000}\right)^{0.8} \times 1100 \quad ,$$

where

k = thermal conductivity in Btu/hr-ft-F

D_H = diameter of the pipe in ft

Pr is the Prandtl number

and Re_H is the Reynolds number, based on D_H.

The fouling factor is assumed to be 0.0005 and the wall resistance is about 0.0003 hr-ft^2-F/Btu. The heat transfer coefficient h_{SS} on the boiling side of the tubing can then be well estimated from:

$$\frac{1}{U} = 0.0005 + 0.0003 + 0.0009 \left(\frac{1000}{\dot{m}_{HW}}\right)^{0.8} + \frac{1}{h_{SS}}$$

or

$$h_{SS} = \left[\frac{1}{U} - 0.0008 - 0.0009 \left(\frac{1000}{\dot{m}_{HW}} \right)^{0.8} \right]^{-1} .$$

It turns out that $1/h_{SS}$ is of the order of $1/U$, which is about five times larger than the two remaining terms combined. Therefore an error of even ± 50% in the two remaining terms results in an error of only ± 10% in h_{SS}.

The data in Fig. 7 show definitely that h_{SS} does not correlate with $(T_{wall} - T_{solution})$ as it should if the heat transfer rates were dominated by pool boiling heat transfer. In fact, as will be shown below, h_{SS} correlates quite well with the average solution rate in the generator per hot water coil, $\dot{m}_S$, where $\dot{m}_S = \frac{1}{2}(\dot{m}_{WS} + \dot{m}_{SS})/(4 \text{ hot water coils})$. This implies that the heat is transferred by conduction and convection to the free surface of the solution layers formed over the coils where boiling occurs.

3.5.2. A correlation for h_{SS} based on forced convection

A classical correlation for h_{SS} can be expressed in terms of the Nusselt number Nu, the Prandtl number Pr, and the Reynolds number Re:

$$Nu = C\, Pr^{0.4}\, Re^{n} , \qquad (4)$$

where C and n are constants fitting the data points; the relationship between Nu and h_{SS} involves the thermal conductivity k and the tube diameter D:

$$h_{SS} = \frac{k}{D} Nu .$$

The flow over the external surface of the hot water coils is quite complicated since it is a combination of a flow along the inclined tubes and a flow normal to the tube. The solution seems to flow along the inclined

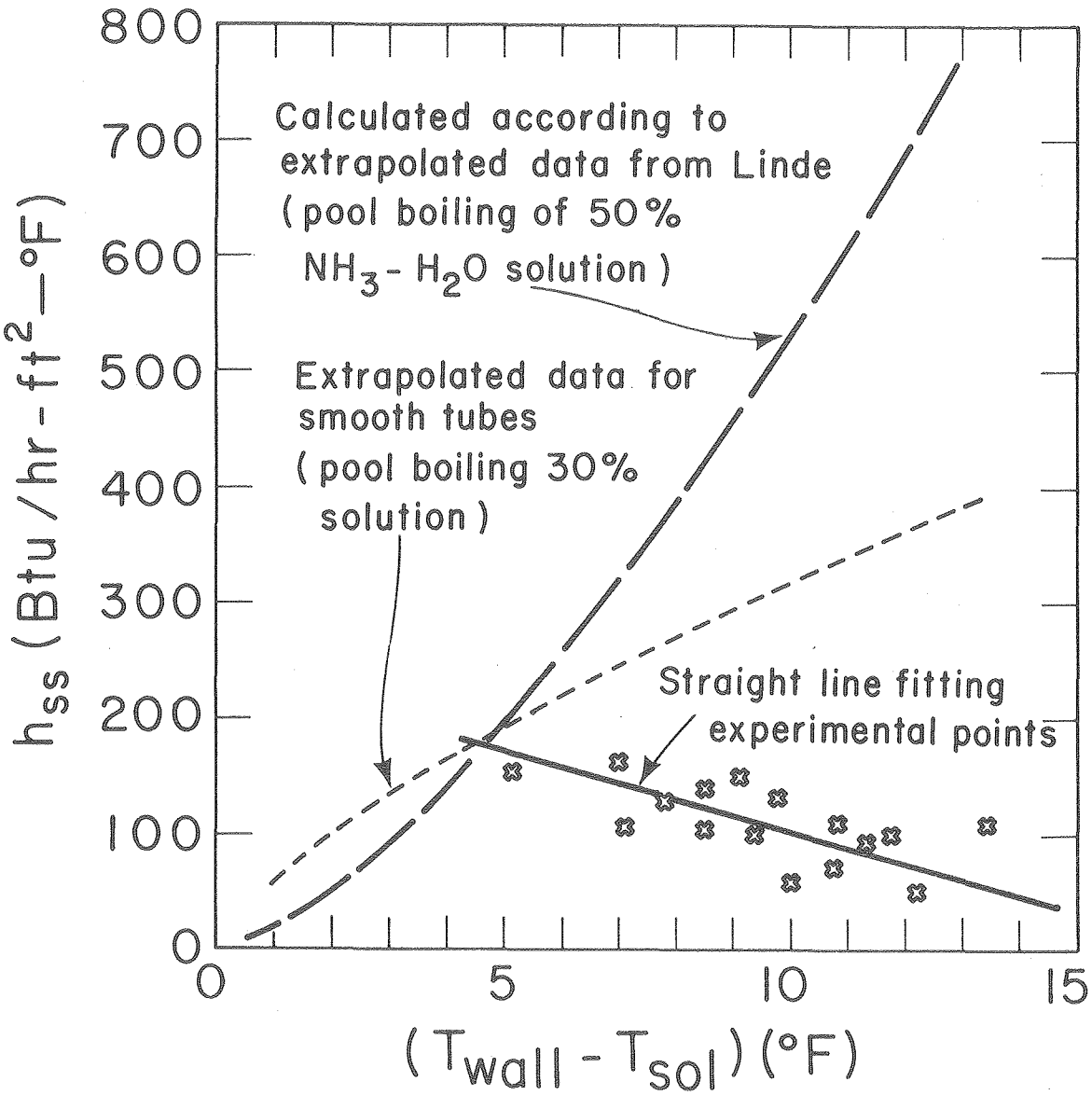

XBL 771-144

Fig. 7. Comparison of experimental results for heat transfer coefficients with values calculated assuming pool boiling.

tubes for some distance and then accumulates into a large drop and falls to the helical tube below. The pall rings break up the drops and distribute them randomly on the surface of the tube below. It is possible that the flow pattern is governed mainly by the diameter of the tube. Therefore it is assumed that the significant dimension is the tube outside diameter D, and the correlation is taken as:

$$Nu_D = C\ Pr^{0.4}\ Re_D^n \quad .$$

The properties of the solution are taken to be (for $170 < T < 200°F$):

$$\mu = 0.83 \text{ lbm/ft-hr}$$

$$Cp = 1.14 \text{ Btu/lbm-F}$$

$$k = 0.31 \text{ Btu/hr-ft-F}$$

$$\rho = 50 \text{ lbs/ft}^3$$

$$D = 0.0625 \text{ ft}$$

$$Pr^{0.4} = 1.55$$

$Re_D = \dot{m}_S/D\mu = 19.3\ \dot{m}_S$ (where $\dot{m}_S$ is the mass flow rate per coil in lbs/hr; there were four coils)

$Nu_D = h_{SS}\ D/k = 0.2\ h_{SS}$ (with h_{SS} in Btu/hr-ft^2-F)

The values of C and n are calculated using the average data points ($h_{SS} = 105$, $\dot{m}_S = 110$) and ($h_{SS} = 164$; $\dot{m}_S = 182.5$):

$$C = 0.016$$

$$n = 0.88$$

Then

$$Nu_D = 0.016\ Pr^{0.4}\ Re_D^{0.88} \quad . \qquad (5)$$

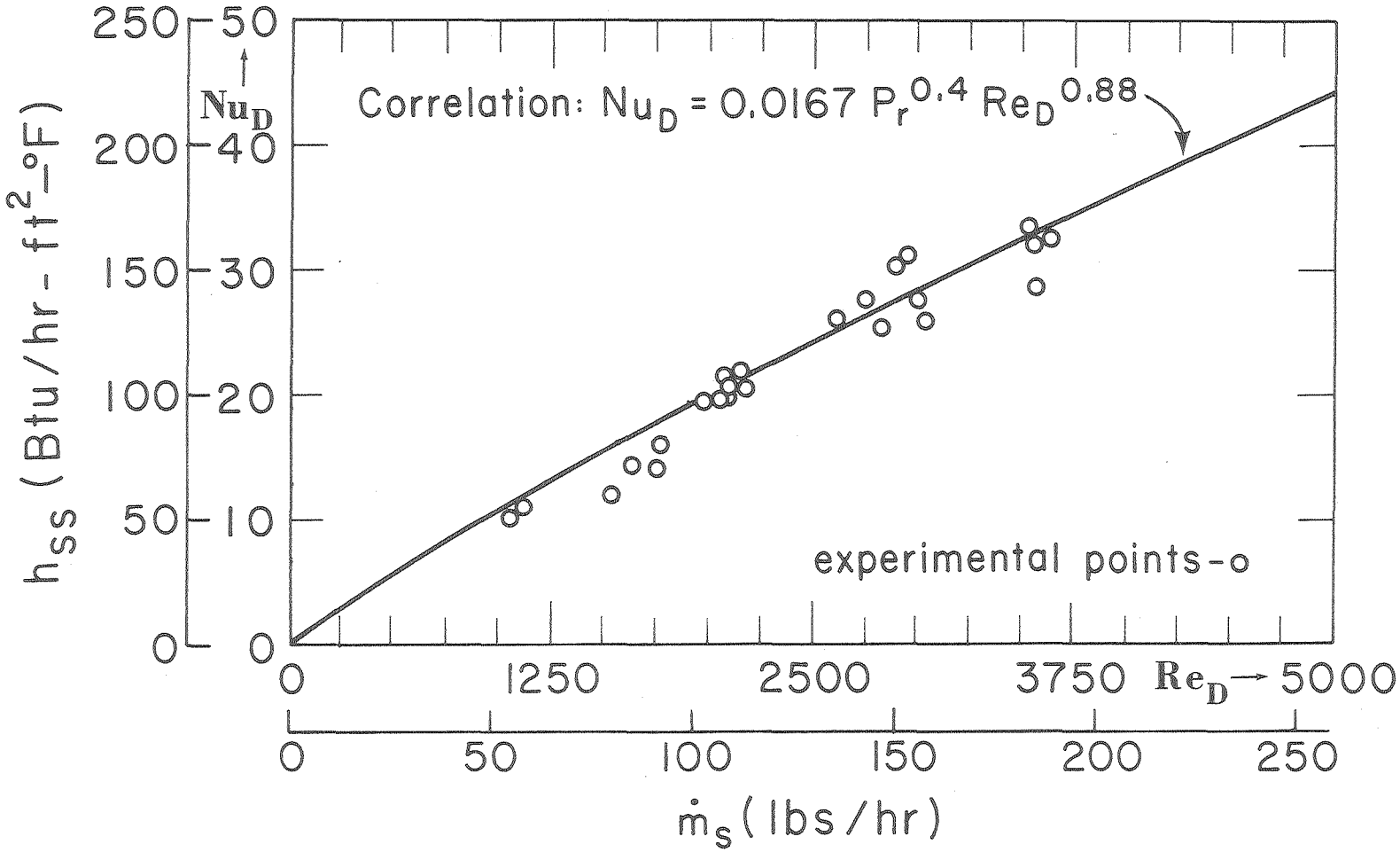

XBL 771-143

Fig. 8. Correlation of the heat transfer coefficient h_{ss} and the average solution flow rate $\dot{m}_s$ over each hot water coil in the generator.

Figure 8 shows that this correlation fits the experimental data.

Thus the heat transfer in the generator is dominated by the forced convection flow of solution over the hot water coil, rather than by enhanced pool boiling at the surface of the coil. It follows that the use of porous surface coating on the coil was not warranted for our application. Subsequent generator designs should use ordinary smooth-wall tubing and forced convection, with the accompanying material cost savings.

4. DISCUSSION OF THE PERFORMANCE OF THE SYSTEM

4.1 Estimation of the Theoretical Maximum Coefficient of Performance

It is desirable to investigate the influence of the various components of an absorption system on its overall performance. The parameter most commonly used to express the performance of a heat-driven refrigeration system is the ratio of the cooling effect q_E to the heat input q_G. This ratio is called the coefficient of performance or COP.

The maximum COP of a system depends on the configuration of the circuits for flow of refrigerant and solutions. The configuration of the system shown in Fig. 9 is used here for the estimation of the maximum COP theoretically achievable. This configuration is the same as that of Figs. 3 and 4. (Note that the solution coil in the absorber is by-passed.)

The maximum COP is attained when all components of the system are assumed to have infinite heat transfer area and are well insulated. Flow friction is also assumed to be negligible.

Considering a control volume enclosing the rectifier, the preheater, and the generator, the heat input q_G to the system is:

$$q_G = \dot{m}_1 h_1 + \dot{m}_{20} h_{20} - \dot{m}_{12} h_{12} \quad .$$

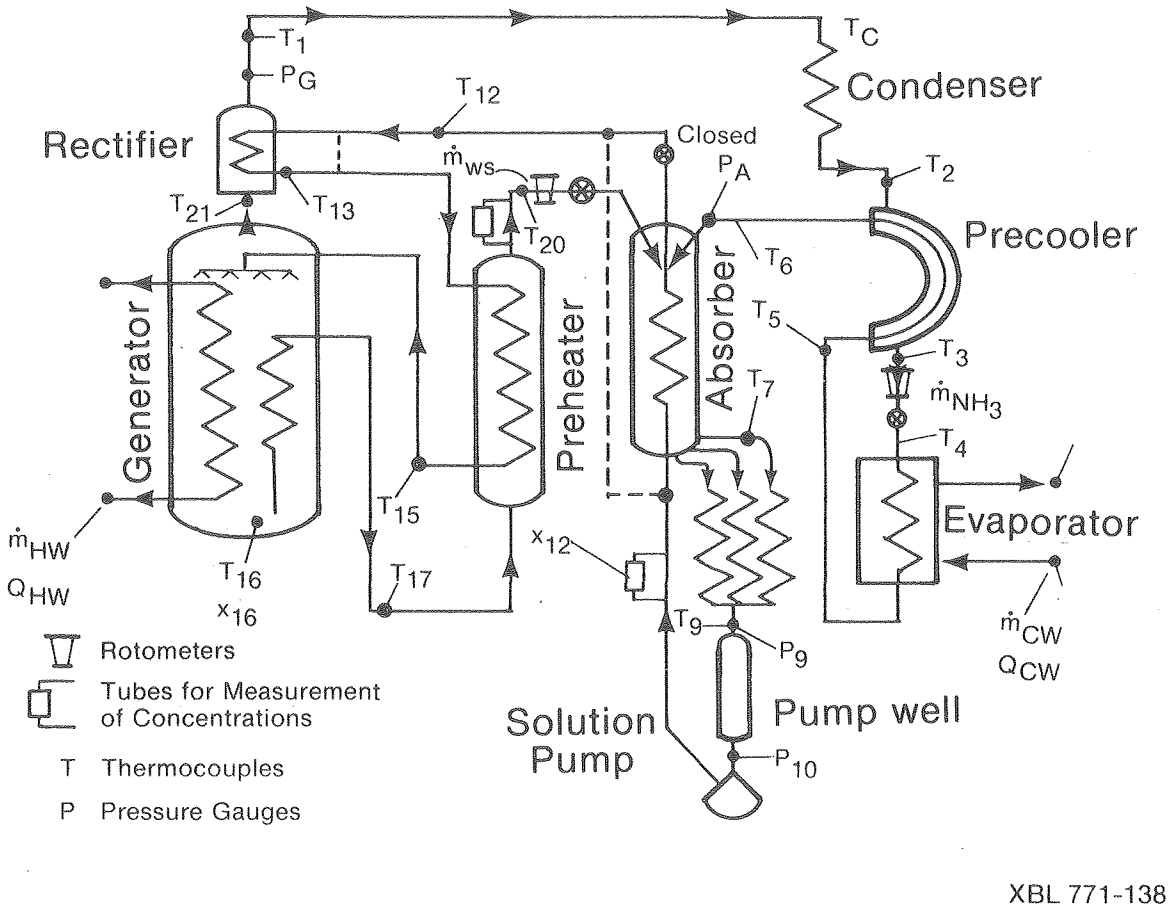

Fig. 9. Configuration of the system used to estimate the COP.

The total mass balance and the mass balance of the water give (neglecting the water content of $\dot{m}_1$):

$$\dot{m}_1 = \dot{m}_{20} \frac{x_{12} - x_{20}}{1 - x_{12}} = \dot{m}_{12} \frac{x_{12} - x_{20}}{1 - x_{20}} .$$

The symbols are:

$\dot{m}$ = mass flow rates

h = enthalpies

x = concentrations: weight of NH_3 per weight of solution.

The subscripts indicate the measurement locations in the system (see Fig. 9). Thus

$$q_G = \dot{m}_1 \left[(h_1 - h_{12}) - (h_{12} - h_{20}) \frac{1 - x_{12}}{x_{12} - x_{20}} \right] \tag{6}$$

The energy balance around the evaporator and precooler gives:

$$q_E = \dot{m}_1 (h_6 - h_2) . \tag{7}$$

Therefore:

$$COP = \frac{h_6 - h_2}{(h_1 - h_{12}) - (1 - x_{12}) \frac{h_{12} - h_{20}}{x_{12} - x_{20}}} \tag{8}$$

For infinitely large heat exchange surfaces, the temperatures are:

$T_1 = T_{12}$

$T_2 = T_6$

$T_{13} = T_{20}$

$T_2 = T_C$, condensing temperature $= T_{\text{cooling air}}$

and $T_{12} = T_A$, absorbing temperature $= T_{\text{cooling air}}$

so:

$$T_1 = T_{12} = T_2 = T_6 = T_C = T_A = T_{air} \quad ,$$

and

$$COP_{max} = \frac{(h_{v,E} - h_{\ell,C})}{(h_{v,G} - h_{SS}) - (1 - x_S)\dfrac{h_{SS} - h_{20}}{x_S - x_W}} \tag{9}$$

where

$h_{v,E}$ is the enthalpy of superheated NH_3 vapor at evaporator pressure P_E and T_{air}

$h_{\ell,C}$ is the enthalpy of saturated liquid NH_3 at T_{air}

$h_{v,G}$ is the enthalpy of the vapor at the generator pressure P_G and T_{air}

h_{SS} is the enthalpy of the saturated strong solution at P_E and T_{air}

x_S and x_W are the concentrations of the strong and weak solutions.

It is clear that given values for T_{air} (which defines P_G) and T_E (which defines P_E), the maximum COP depends on the quantity:

$$(1 - x_S)\ \frac{h_{SS} - h_{20}}{x_S - x_W} \quad ,$$

which in turn depends on the generator temperature T_G and the preheater effectiveness.

At most the preheater can make $T_{20} = T_{13}$. Due to the configuration of the system, $T_{13} > T_{12}$. At small $\Delta x = x_S - x_W$, the enthalpies of the solutions at the same temperature are approximately equal, so $h_{13} \simeq h_{20} > h_{12} = h_{SS}$, or $(h_{SS} - h_{20}) < 0$. Thus the COP_{max} is always less than:

$$COP_{max} < \frac{h_{v,E} - h_{\ell,C}}{h_{v,G} - h_{SS}} \quad .$$

If the rectifier and the preheater were combined into a "three-way" heat exchanger, T_{20} could be made equal to T_{12} as shown in the diagram below:

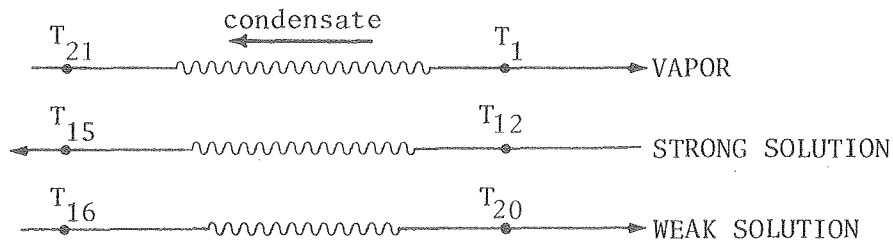

and $(h_{12} - h_{20})$ could approach zero in the limit $\Delta x \to 0$.

With the preheater and rectifier separated, the strong solution cannot absorb both the heat in the vapor and in the weak solution. Only a fraction $(1 - \dot{m}_{WS}/\dot{m}_{SS})$ of the heat in the temperature range $(T_{13} - T_{12})$ across the rectifier is recovered, since the heat gain from the vapor is $\dot{m}_{SS}Cp(T_{13} - T_{12})$ and the heat that cannot be recovered from the weak solution is $\dot{m}_{WS}Cp(T_{20} - T_{12}) = \dot{m}_{WS}Cp(T_{13} - T_{12})$.

Now, assume $T_{12} \simeq T_{20}$; then,

$$\frac{h_{12} - h_{20}}{x_{12} - x_{20}} \simeq \left(\frac{\partial h}{\partial x}\right)_{\text{constant T,saturated}} .$$

This derivative is the slope of the line of constant temperature in the diagram of saturated properties of the ammonia-water. This slope can be negative or positive for the case of the "three-way" heat exchanger. It is desirable to operate at positive slopes, for $-(1 - x_{12})\partial h/\partial x$ would then be negative and the COP would be improved.

For a concentration of the weak solution, x_W, greater than about 0.40, $\partial h/\partial x$ is $\geqslant 0$.

With the assumption of $T_{12} \simeq T_{20}$, the following approximation can be

made, using a quadratic to approximate the properties of the solution:

$$(h_{v,G} - h_{SS}) - (1 - x_S)\frac{h_{SS} - h_{WS}}{x_S - x_W} \simeq$$

$$970 - 0.62\ T_A - (x_W + x_S - x_W x_S)(370 + 0.75\ T_A)\ . \tag{10}$$

where T_A is the absorbing temperature (in °F), and x_W and x_S are the weak and strong concentrations. The above relation applies for:

$$0.4 < x_W < x_S < 0.6$$

$$80 < T_C \leqslant T_A < 120\ F$$

The following approximation:

$$h_{v,E} - h_{e,C} = 580 - 0.56\ T_C - 0.39\ T_E$$

applies for:

$$20 < T_E < 60\ F$$

$$80 < T_C < 120\ F$$

All approximations differ from the values obtained from the tables by less than 0.5%. Now:

$$COP_{max} = \frac{580 - 0.56\ T_C - 0.39\ T_E}{970 - 0.62\ T_A - (x_W + x_S - x_W x_S)(370 + 0.75\ T_A)} \tag{11}$$

As long as T_C, T_E, T_A, and T_G are such that the condition $x_W < x_S$ is satisfied, the COP_{max} depends very little on these temperatures. A variation of these temperatures by ± 20° F changes the COP_{max} only by about about ± 10%.

Figure 10 shows a plot of this maximum COP as a function of the generator temperature [calculated with equation (9)] for a system with

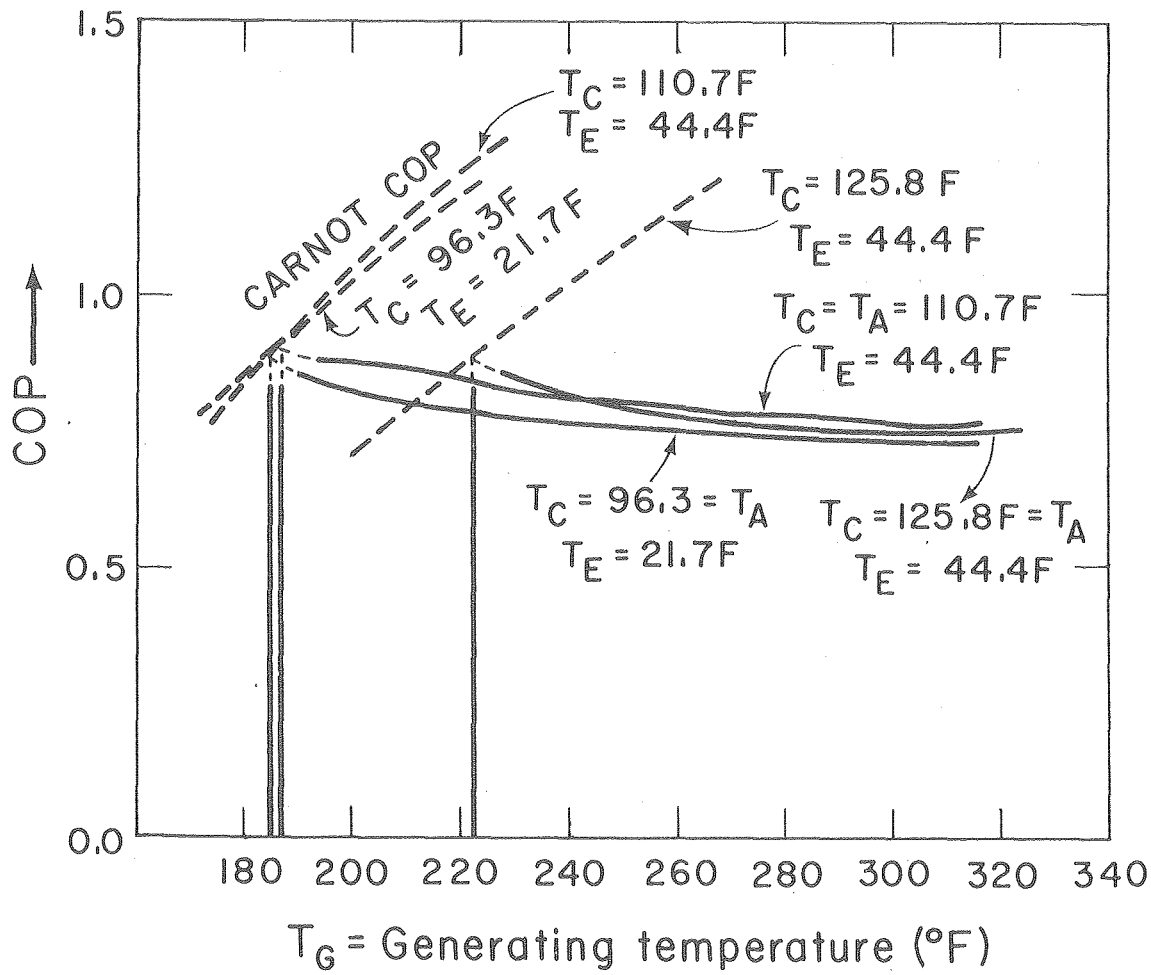

XBL 771-141

Fig. 10. Theoretical max COP for NH_3-H_2O absorption cycle (single stage) at different operating temperatures (equation 9).

infinite heat exchangers including a preheater-rectifier combination heat exchanger for $T_{20} = T_{12}$. It can be seen, from Fig. 10, that the COP_{max} is decreasing at higher T_G and that the COP_{max} approaches the COP_{Carnot} only near the cut-off point. This implies that theoretically the single stage ammonia-water absorption refrigeration system works efficiently only at low generation temperature T_G.

4.2 Practical COP

The calculation of COP_{max} in the previous section is now modified by including the effects of finite size of heat exchanger surfaces in reducing q_E and increasing q_G.

4.2.1. Influence of the precooler

Due to the finite size of the precooler, not all the coldness of the vapor from the evaporator is available to cool the liquid ammonia leaving the condensor. If the effectiveness of the precooler is e_{PC}, then the loss of cooling effect in the evaporator is:

$$(1 - e_{PC})0.64(T_C - T_E) \ , \quad \text{Btu per pound of } NH_3 \ .$$

A precooler effectiveness of 0.75 is fairly inexpensive to realize; the loss could be:

$$0.16\ T_C - 0.16\ T_E \ , \quad \text{Btu per lb of } NH_3 \ . \tag{12}$$

4.2.2. Influence of the preheater

If the effectiveness of the preheater is e_{PH}, the heat recovered from the weak solution could be only $e_{PH}\ \dot{m}_{WS}C_{WS}(T_G - T_A)$; the extra heat

requirement could then be, at the worst:

$$(1 - e_{PH})\dot{m}_{SS}C_{SS}(T_G - T_A)/\dot{m}_{NH_3} \quad , \quad \text{Btu per lb of } NH_3 \quad ,$$

where the subscripts WS and SS refer to the weak and strong solutions, and the C's are the specific heats at constant pressure.

With: $\dot{m}_{SS}/\dot{m}_{NH_3} = [1 - x_W]/[x_S - x_W]$, the extra heat required in the generator can be written:

$$(1 - e_{PH})(T_G - T_A)C_{SS} \frac{1 - x_W}{x_S - x_W} \quad , \quad \text{Btu per lb of } NH_3 \qquad (13)$$

4.2.3. Influence of the rectifier

As arranged separately from the preheater, the rectifier introduces an extra heat requirement of about $\dot{m}_{WS}/\dot{m}_{NH_3}\ C_{WS}(T_{13} - T_{12})$, Btu per lb of NH_3, which represents the heat that cannot be recovered from the weak solution.

Since

$$(T_{13} - T_{12}) = \frac{\dot{m}_{NH_3}}{\dot{m}_{SS}} \frac{C_g}{C_{SS}} (T'_G - T_A) \quad ,$$

this loss is approximately $C_g(T'_G - T_A) \simeq 1.1(T'_G - T_A)$, where C_g is the equivalent specific heat of the vapor (including the condensation of liquid) and T'_G is the temperature of the vapor leaving the generator which can also be the saturated temperature of the strong solution at the pressure of the generator.

To simplify the calculations, this loss is approximated by $0.8(T_G - T_A)$, Btu per lb of NH_3.

With a "three-way" preheater, the strong solution could recover both the heat in the vapor and the heat from the weak solution. Then the loss

$0.8(T_G - T_A)$ would be eliminated and the COP_{max} could be expressed as in equation (11), which applies for the case with $T_1 = T_{12}$ and $T_{20} = T_{12}$.

4.2.4. Influence of the analyzer

The analyzer (i.e., the weak solution recirculation coil in the generator) can be considered as an extension of the preheater; therefore its effect is to increase e_{PH}.

Referring to Fig. 9, the effectiveness of the preheater should be evaluated as:

$$e_{PH} = \frac{T_{16} - T_{20}}{T_{16} - T_{13}} \quad \text{instead of} \quad \frac{T_{17} - T_{20}}{T_{17} - T_{13}} \quad . \tag{14}$$

4.2.5. Influence of the strong solution recirculation coil in the absorber

The influence of this coil (which was part of the unit in its gas-fired configuration) is rather small for operation from flat-plate solar collectors. Two cases will now be considered to examine the benefit of a strong solution recirculation coil.

First, consider the case of a large preheater and a large recirculation coil, such that the weak solution can be cooled close to the temperature of the strong solution leaving the recirculation coil, $T'_A > T_A$. The heat received by the strong solution along the preheater is then the heat given up by the weak solution,

$$\dot{m}_{WS} C_{WS} \, (T_G - T'_A) \quad .$$

The amount of heat received by the strong solution along the recirculation

coil is: $\dot{m}_{SS}C_{SS}(T'_A - T_A)$, when the strong solution does not boil in the recirculation coil. When boiling occurs in this recirculation coil, the amount of heat received by the strong solution along this coil would be:

$$\dot{m}_{SS}C_{SS}(T'_G - T_A) + \dot{m}_{SS}C'_{SS}(T'_A - T'_G)$$

where T'_G is the saturation temperature of the strong solution at P_G and C'_{SS} is the equivalent specific heat of the strong solution (C'_{SS} is about 4 Btu/lb-°F at $x_{SS} = 0.4$ and C_{SS} is about 1.135 at $x_{SS} = 0.4$).

Since with the recirculation coil the strong solution leaving the recirculation coil is at T'_A rather than T_A, the vapor leaving the rectifier can only be cooled to T'_A; therefore the total possible heat recovery is:

$$\dot{m}_{WS}C_{WS}(T_G - T'_A) + \dot{m}_{NH_3}C_g(T_G - T'_A) + \dot{m}_{SS}C_{SS}(T'_G - T_A) + \dot{m}_{SS}C'_{SS}(T'_A - T'_G) \quad .$$

(Note that if there is no boiling in the recirculation coil, $T'_G > T'_A$ then take $T'_G = T'_A$). Depending on T'_A, C_g can be from 1.2 to 0.65.

Now consider the case of a large preheater without a recirculation coil. The weak solution and the vapor can be cooled to T_A; therefore the amount of heat received by the strong solution along the preheater-rectifier is:

$$\dot{m}_{WS}C_{WS}(T_G - T_A) + \dot{m}_{NH_3}C_g(T_G - T_A) \quad .$$

The net gain of the first case over the second is

$$\dot{m}_{NH_3}(C_{SS} - C_g)(T'_A - T_A) + \dot{m}_{SS}(C'_{SS} - C_{SS})(T'_A - T'_G) \quad . \tag{15}$$

The second term of equation (15) can be written as a heat gain per pound of ammonia vapor generated:

$$\frac{1 - x_W}{x_S - x_W}(C'_{SS} - C_{SS})(T'_A - T'_G) \quad .$$

(Note that if $T'_A < T'_G$, then take $(T'_A - T'_G) = 0$.) In a practical gas-fired system, with T_G of the order of 350 F, $T'_A - T'_G$ is about 10 F, $(C'_{SS} - C_{SS}) \simeq 3.0$ and $(1-x_W)/(x_S-x_W) = 3$, this second term is about 90 Btu/lb of NH_3. However, in operation with solar flat-plate collectors, the first term is about 4 Btu/lb of NH_3 and the second term is zero. (The first term is also about 4 Btu/lb of NH_3 for gas-fired operation.)

So the recirculation coil is useful only at high T_G, and for solar flat-plate collectors, this coil is not necessary.

4.2.6. Calculation of Practical COP

Now, the practical COP can be written, for the system configuration of Fig. 9, as:

$$COP = \frac{q_E}{q_G} \pm 1\% \qquad (16)$$

where

$$q_E = 580 - 0.72\ T_C - 0.23\ T_E$$

and

$$q_G = 970 - 0.62\ T_A - (x_W + x_S - x_W x_S)(370 + 0.75\ T_A) + \left[1.14(1 - e_{PH})(1 - x_W) / (x_S - x_W) + 0.8\right](T_G - T_A)$$

(See Appendix II, Table 8 and Fig. 11 for comparison of equation (16) with experimental data.) Limiting the range of operation to:

$$95 < T_C < T_A < 115°F$$

$$180 < T_G < 195°F$$

$$40 < T_E < 50°F$$

$$0.46 < x_W < x_S < 0.56$$

$$\Delta X > 0.02$$

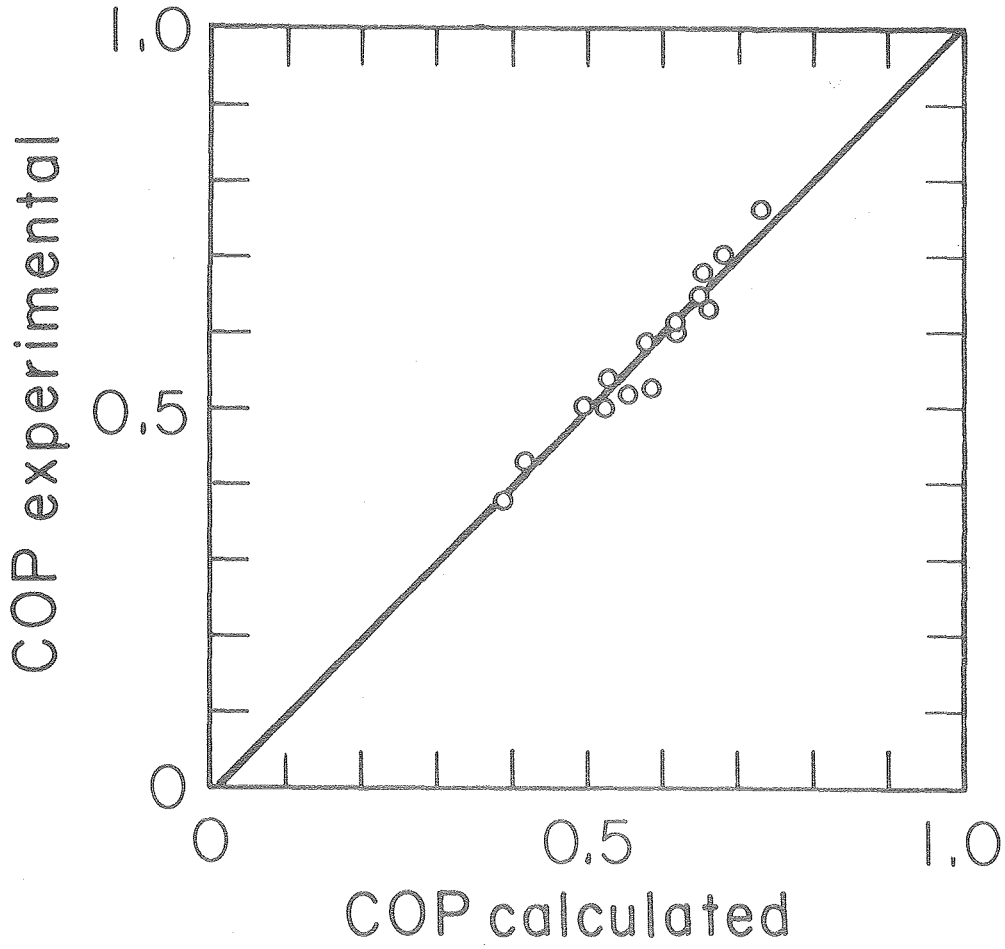

XBL 771-146

Fig. 11. Experimental verification of equation 16.

$$COP = \frac{494}{564 + 220\ \Delta x + (70 + 325\ \Delta x)[0.57(1 - e_{PH})/\Delta x + 0.8]} \pm 3\% \qquad (17)$$

Figure 12 shows how the COP varies with e_{PH} and Δx according to equation (17).

4.3 Possible Range of Operation

The possible evaporating temperatures T_E of the ammonia-water system can be written as

$$T_E = 3.2 + 1.82\ T_C - 0.852\ T_G + (1.07 - 0.0097\ T_E)(\Delta P + a\Delta x) \quad , \qquad (18)$$

where ΔP is the pressure drop across the absorber, $\Delta x = x_S - x_W$, and

$$a = \frac{1}{\Delta x} \int_{x_W}^{x_S} \left(\frac{\partial P_A}{\partial x}\right)_{T_A} dx \quad . \qquad (19)$$

The quantity a can be approximated by $(\partial P/\partial x)_{T_A,\text{saturated}}$ evaluated at $\frac{1}{2}(x_S + x_W)$; a is then approximately $5T_A - 140 - (T_A - 40)(1.82 - 0.018\ T_G + 0.021\ T_E)^2$ (in fact taking $a = 350$ psi is satisfactory).

Equation (18) is obtained by the following considerations:

i. The relation $T_E = 3.2 + 1.82\ T_C - 0.852\ T_G \pm 0.2$ F is a fit to the plot of T_E versus T_C $(=T_A)$ and T_G at the cut-off conditions, $\Delta x = 0$.

(NOTE: This relation for the cut-off temperatures can also be obtained from the fact that the maximum theoretical COP approaches the Carnot COP at cut-off:

$$\frac{(T_G - T_C)(T_E + 460)}{(T_G + 460)(T_C - T_E)} = COP_{max} \simeq 1.076 - 0.0025(T_C - T_E) \quad , \qquad (20)$$

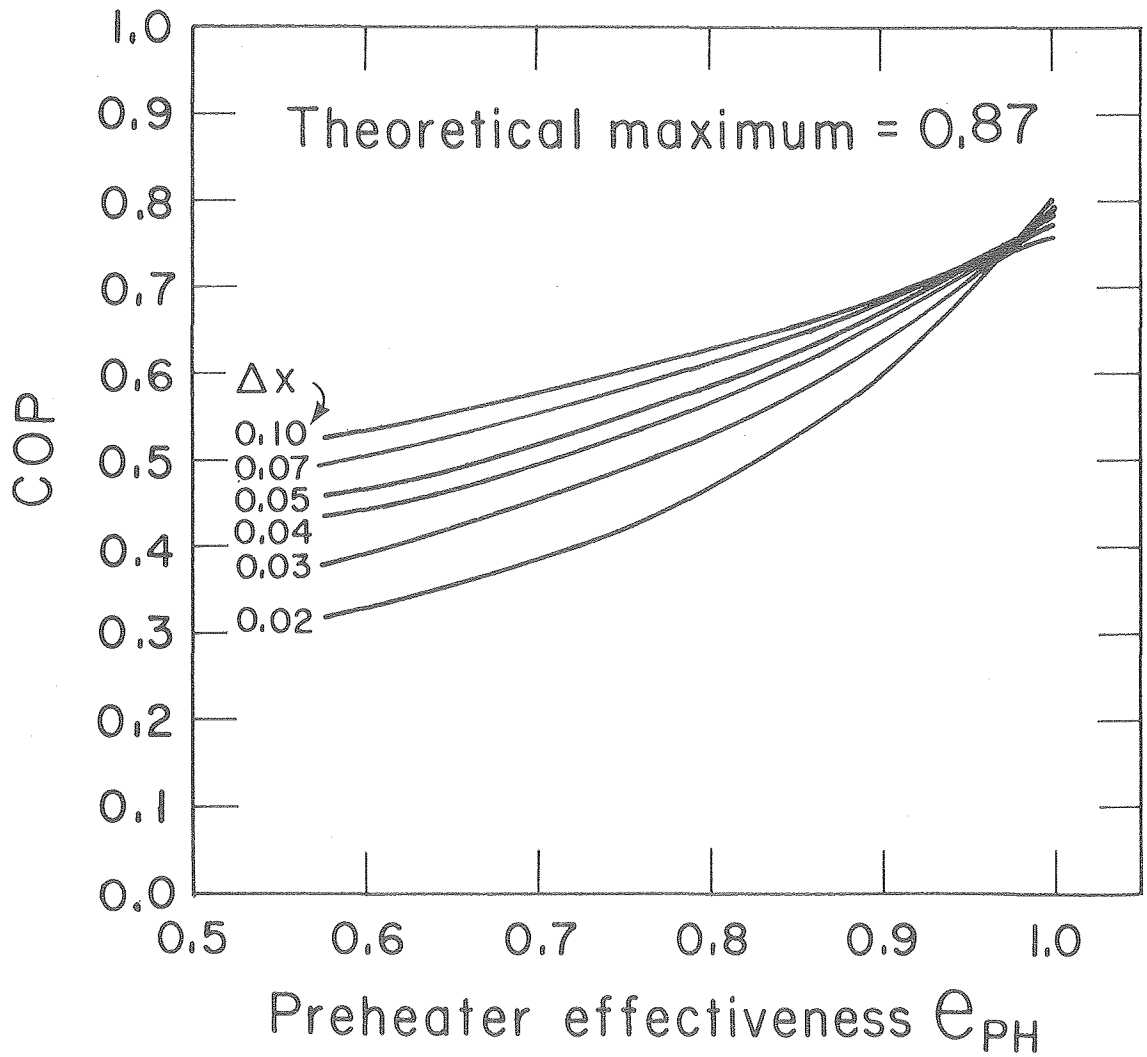

XBL 771-145

Fig. 12. COP as a function of the preheater effectiveness and of the concentration difference $\Delta x = x_S - x_W$ (equation 17).

ii. The term $(1.07 - 0.0097\ T_E)\Delta P$ represents the increase of T_E due to an increase in the absorber pressure P_A to compensate for the pressure drop ΔP across the absorber as discussed in Section 3.4. The factor $(1.07 - 0.0097\ T_E)$ is a fitting of data for (dT_E/dP_E) versus T_E for saturated NH_3 for $30 < T_E < 55°F$.

iii. The factor $(1.07 - 0.0097\ T_E)a\Delta x$ represents the increase of T_E because $\Delta x \neq 0$ or $x_S \neq x_W$. With T_A maintained constant, in order to increase x_S by an amount of Δx above x_W, the pressure in the absorber must be increased; therefore T_E also increases. The change of T_E due to Δx is:

$$\frac{dT_E}{dx} = \left(\frac{dT_E}{dP_E}\right)_{sat.NH_3} \left(\frac{\partial P}{\partial x}\right)_{T_A,sat.sol.} = (1.07 - 0.0097\ T_E)\cdot a$$

(See Appendix II, Table 10 for the comparison of equation (18) with experimental data.)

Now, if T_E is fixed at 45°F and $\Delta P = 3$ psi, equation (18) becomes:

$$39.9 = 1.82\ T_C - 0.852\ T_G + 0.63\ a\Delta x \qquad (21)$$

Figure 13 is the graphical representation of equation (21). Figure 13 shows that, for $T_E = 45°F$ and $180 < T_G < 190°F$, the condensing and absorbing temperatures should be below 110°F. When T_C and T_A are high, it is necessary to operate at low Δx, i.e., high circulation ratios.

The penalties for operation at low Δx are a high pumping power and a low COP. Figure 12 shows how the COP decreases at low Δx for a constant preheater effectiveness. To increase the COP at low Δx, a larger preheater is needed.

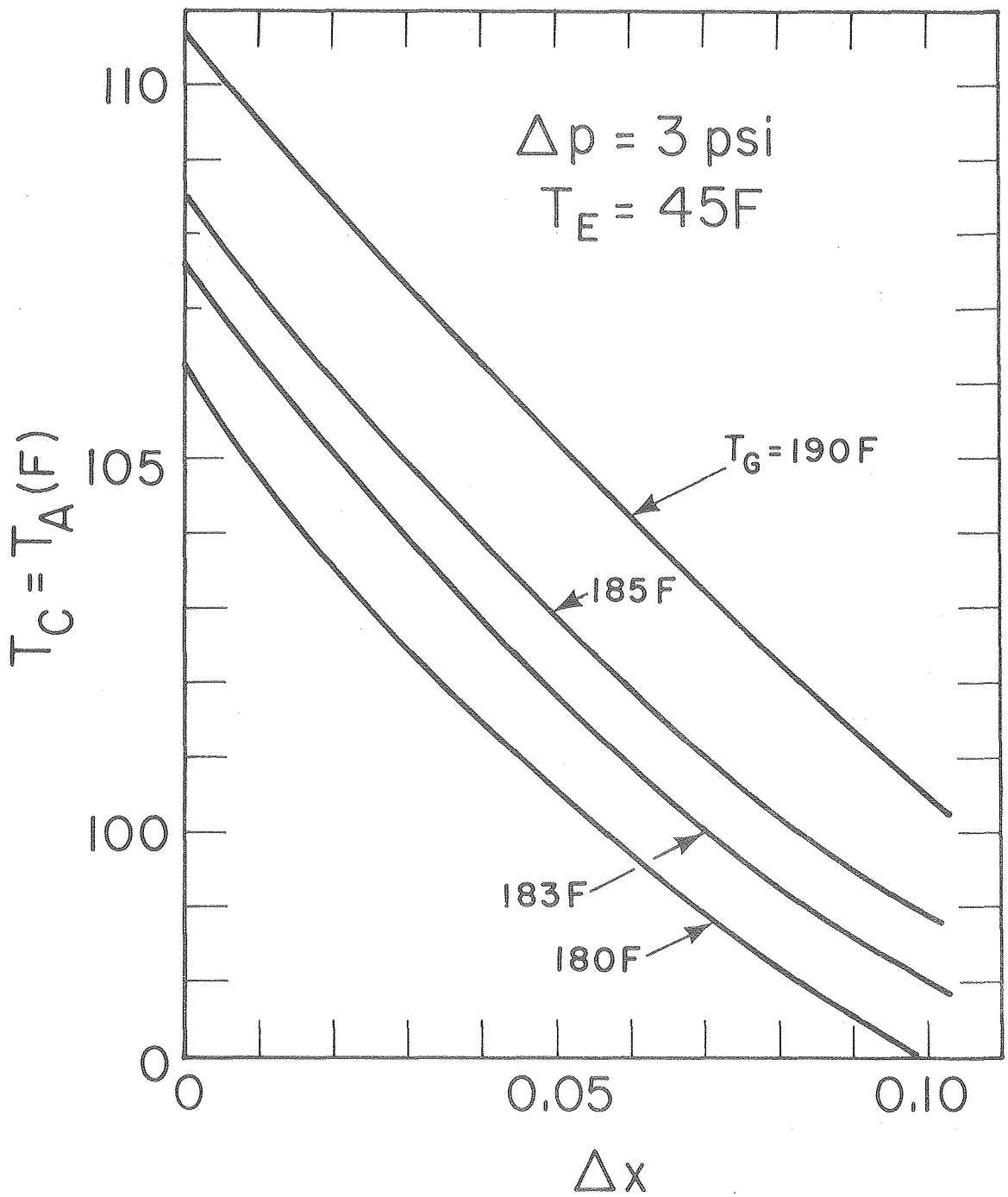

XBL 771-148

Fig. 13. Possible operating range of an ammonia-water absorption system at a fixed evaporating temperature of 45°F and a 3 psi pressure drop across the absorber.

The pumping power for the strong solution can be estimated by:

$$\dot{W} = \dot{m}_{SS} \, (P_G - P_A)/\rho_{SS} e_P \tag{22}$$

where ρ_{SS} is the specific mass of the strong solution, $(P_G - P_A)$ is the pressure difference between the generator and absorber, and e_P is the efficiency of the pumps. To estimate how $\dot{W}$ varies with Δx, the following values can be used:

$$\rho_{SS} = 50 \text{ lbm/ft}^3$$

$$P_G - p_A \simeq 160 \times 144 \text{ lbf/ft}^2$$

$$\dot{m}_{SS} \simeq 0.5 \, \dot{m}_{NH_3}/\Delta x$$

and

$$\dot{m}_{NH_3} \simeq q_E/505$$

where the number 505 is an approximation to $(h_6 - h_2)$, and the number 0.5 is an approximation to $(1 - xw)$.

so that:

$$\frac{\dot{W}}{q_E} = \frac{1.72 \times 10^{-4}}{e_P \Delta x} \text{ watts per Btu/hr}$$

$$= \frac{2.06}{e_P \Delta x} \text{ watts per ton} \quad . \tag{23}$$

Assuming $e_P = 0.4$ and assuming an arbitrary limit of $q_E/\dot{W} \geqslant 70$ Btu/hr per watt, then Δx is limited to $\Delta x \geqslant 0.03$. (Note that the power of the condensor-absorber fan can require additional electrical power corresponding to 130 Btu/hr per watt.)

Now, let $\Delta x = 0.03$ and $\Delta P = 3$ psi (the value of a is fairly constant and equal to about 350 psi); then equation (18) becomes:

$$T_E = 11.4 + 1.82 \, T_C - 0.852 \, T_G \tag{24}$$

Figure 14 displays equation (24). The region inside the dash-lined trapezoid represents the possible operating conditions for the ammonia-

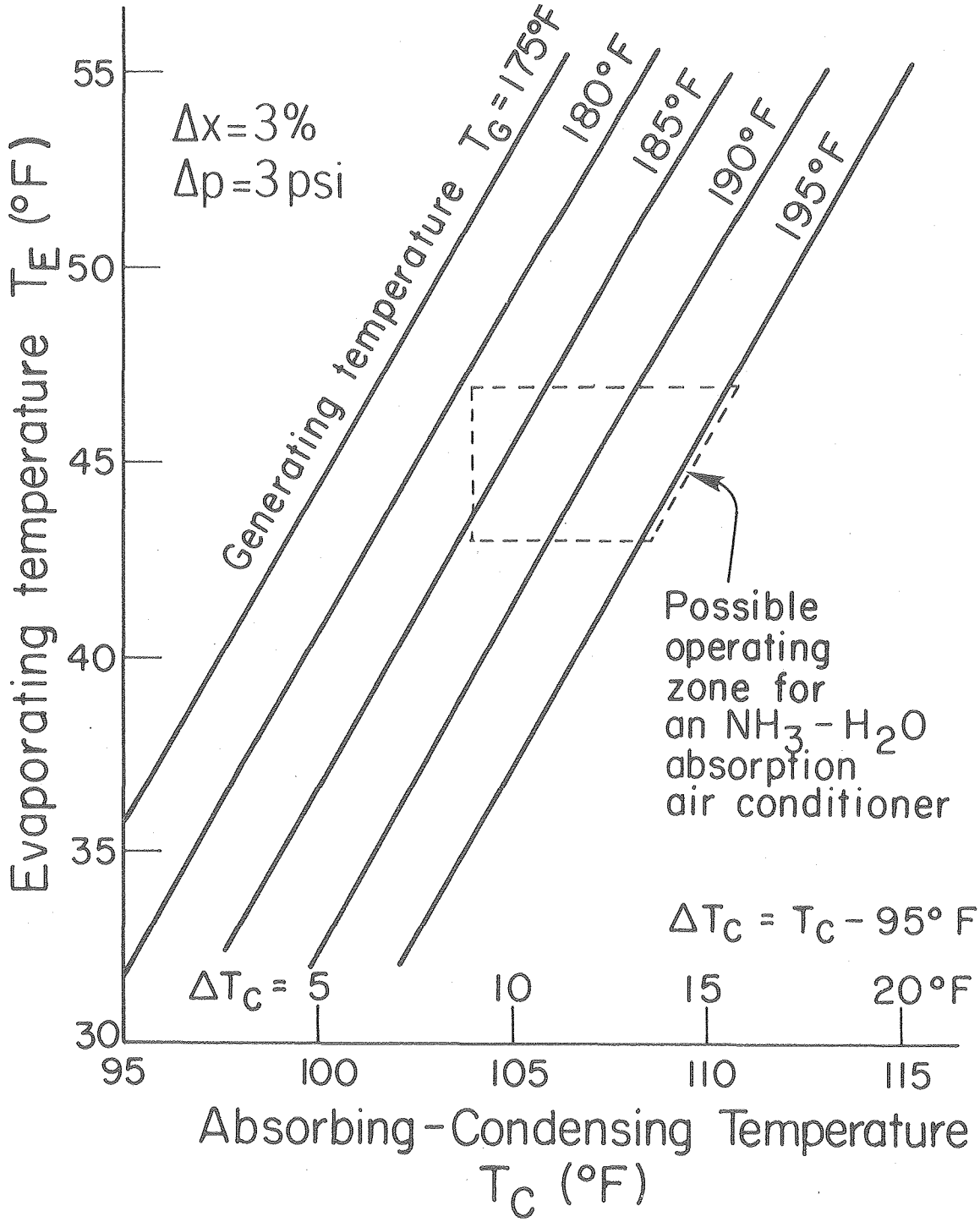

XBL 767-3133

Fig. 14. T_E as a function of T_G and $T_A = T_C$ for a pressure drop across the absorber of 3 psi and a concentration difference of 0.03.

water system. This region is bounded by the following criteria:

i. Solution pumping power less than 0.0143 watt per Btu/hr of cooling load;

ii. Pressure drop across the absorber less than 3 psi;

iii. Temperature approach of the condensor and absorber between 9°F and 15°F above the ambient temperature of 95°F;

iv. Generator temperature less than 196°F;

v. Evaporating temperature between 43° and 47°F;

vi. Preheater effectiveness better than 0.87 for a COP better than 0.6.

Criterion (i) is arbitrary but realistic, since a solution pump with efficiency of more than 0.4 is now available commercially. A rating of 70 Btu/hr per watt for the pumps and another 130 Btu/hr per watt for the fans still yields only a total ratio of about 46 Btu/hr per watt as compared to a ratio of about 8 Btu/hr per watt for an electrically driven compression air conditioner.

Criteria (ii) and (vi) are relatively inexpensive to satisfy by connecting more parallel coils to the absorber, and using the large pressure difference available across the weak solution line to improve the heat transfer rates in the preheater. Since the circulation ratio is high, short parallel coils are sufficient for a complete absorption process.

Criterion (iv) can be satisfied by flat-plate collectors now commercially available. However, a more efficient generator needs to be designed to reduce the temperature approach, $T_{collector} - T_G$.

More efficient air-cooled condensor-absorber coils need to be developed to satisfy criterion (iii). With the conventional finned-tube coils, present practice limits the temperature approach, $\Delta T_C = T_C - T_{air}$, to more than 20°F. To reduce ΔT_C to about 12°F, the size of the coils must be doubled and the fan capacity must also be doubled. With a fan capacity twice as large, the ratio $q_E/\dot{W}$ decreases to 35 Btu/hr per watt instead of 46 as stated in criterion (i). This ratio of 35 may still be acceptable.

Doubling the size of the condensor-absorber can increase the cost of the solar-driven air-conditioner by about 40% as compared to the gas-fired unit of the same cooling capacity. This does not seem to be an attractive proposition, so high priority should be placed on developing new design concepts for the condensor-absorber.

One important consideration in favor of the ammonia-water absorption refrigeration is the possibility of using the unit for heating. The heat source can be either a back-up system, or the solar collectors if the collecting temperature can produce a T_G of 180°F. Figure 14 shows that at $T_G = 180°F$ and $T_C = T_A = 95°F$, the evaporating temperature T_E can be 32°F, which is low enough to absorb heat from an outdoor temperature of about 45°F. With $T_C = T_A = 95°F$, the house air temperature can be heated from 74°F to 86°F at a flow rate equal to the capacity of the condensor-absorber fan.

5. CONCLUSION

Initial testing of an experimental solar-driven ammonia-water absorption system demonstrated stable operation of the system near the cut-off conditions. It was verified that equilibrium thermodynamic properties of the working fluids can be assumed everywhere in the cycle, allowing analytical calculations of the cycle to be used for the prediction of the performance of the system.

Calculations with equations that have been verified experimentally to less than ± 5% error confirmed the feasibility of operation of the system in the following ranges:

$$180 < T_G < 196°F$$

$$43 < T_E < 47°F$$

$$104 < T_C \leqslant T_A < 110°F$$

$$\frac{q_E}{\dot{W}} = \frac{\text{cooling load}}{\text{total mechanical power}} > 35 \text{ Btu/hr per watt}$$

pump efficiency > 40%

COP = 0.65 to 0.70

$$\text{circulation ratio} < 17 \frac{\text{lbs of solution}}{\text{lbs of } NH_3}$$

However, new designs of the generator need to be developed to improve the overall heat transfer coefficient attainable at small size and thus low cost, and also new designs of the condensor-absorber need to be developed to replace the conventional finned-tube coils and lower the cost of attaining T_C, $T_A < 110°F$.

0 0 0 0 4 7 0 3 8 5 4

ACKNOWLEDGMENT

Work performed under the auspices of the U.S. Energy Research and Development Administration, Division of Solar Energy, Heating and Cooling Research and Development Branch.

REFERENCES

(1) "A Solar driven ammonia-water absorption air conditioner", by M. Simmons, R. Wolgast, and M. Wahlig, Lawrence Berkeley Laboratory Report LBL-3293, presented at ISES Meeting in Los Angeles, July-August, 1975.

(2) "Performance of an air-cooled ammonia-water absorption air conditioner at low generator temperatures", by K. Dao, M. Simmons, R. Wolgast, and M. Wahlig, Lawrence Berkeley Laboratory Report LBL-5224, presented at ISES Meeting in Winnipeg, Canada, August 1976.

(3) "Proposed correlation of data for isothermal two-phase, two-component flow in pipes", by R. W. Lockhart and R. C. Martinelli, in Chemical Engineering Progress 45, Jan. 1949, pp. 39-46.

(4) Handbook of Heat Transfer, by W. M. Rohsenow and J. P. Hartnett, McGraw-Hill, Section 14, p. 11.

APPENDIX I. COMPONENT SPECIFICATIONS

Size and Type of the Heat Exchangers Used for the Experimental Unit

Air Cooled Condensor

5/8" steel tubing, 16 gauge wall

Aluminum fins: 0.01" thick, 14 fins per inch of tube length

Fin area/total area = 0.985

Total tube length: 100 ft

Total OD tube area: 14 ft^2

Air Cooled Absorber

Same tubing and fins as condensor

Total tube length: 160 ft

Total OD tube area: 22 ft^2

Total air flow rate for condensor and absorber: 4000 cfm

Rectifier

Tube in shell heat exchanger, one pass

Total tube area: 2.4 ft^2

Tubing: stainless steel 1/4 inch OD

Preheater

Tube in shell heat exchanger, one pass

Total tube area: 22 ft^3

Tubing: stainless steel 1/4 inch OD

(NOTE: Twisted tapes of pitch 2.5" are inserted in all tubes of the rectifier and the preheater.)

Physical Data of the Generator

Water Coils:

Tubing: 3/4 inch OD; 0.584 inch ID, Linde hi-flux tubing

Total length: 184 ft

Total outside surface area: 36 ft^2

Analyzer (solution coil): same tubing; area: 4 ft^2

Shell diameter: 16 inches

Overall height: 72 inches (6 ft)

Packing: 5/8 inch steel pall rings

Water flow rates: up to 5000 lbs/hr (10 gpm)

Solution flow rates: up to 1000 lbs/hr (2.5 gpm)

(NOTE: Twisted tapes of pitch 3" are inserted in all water coils.)

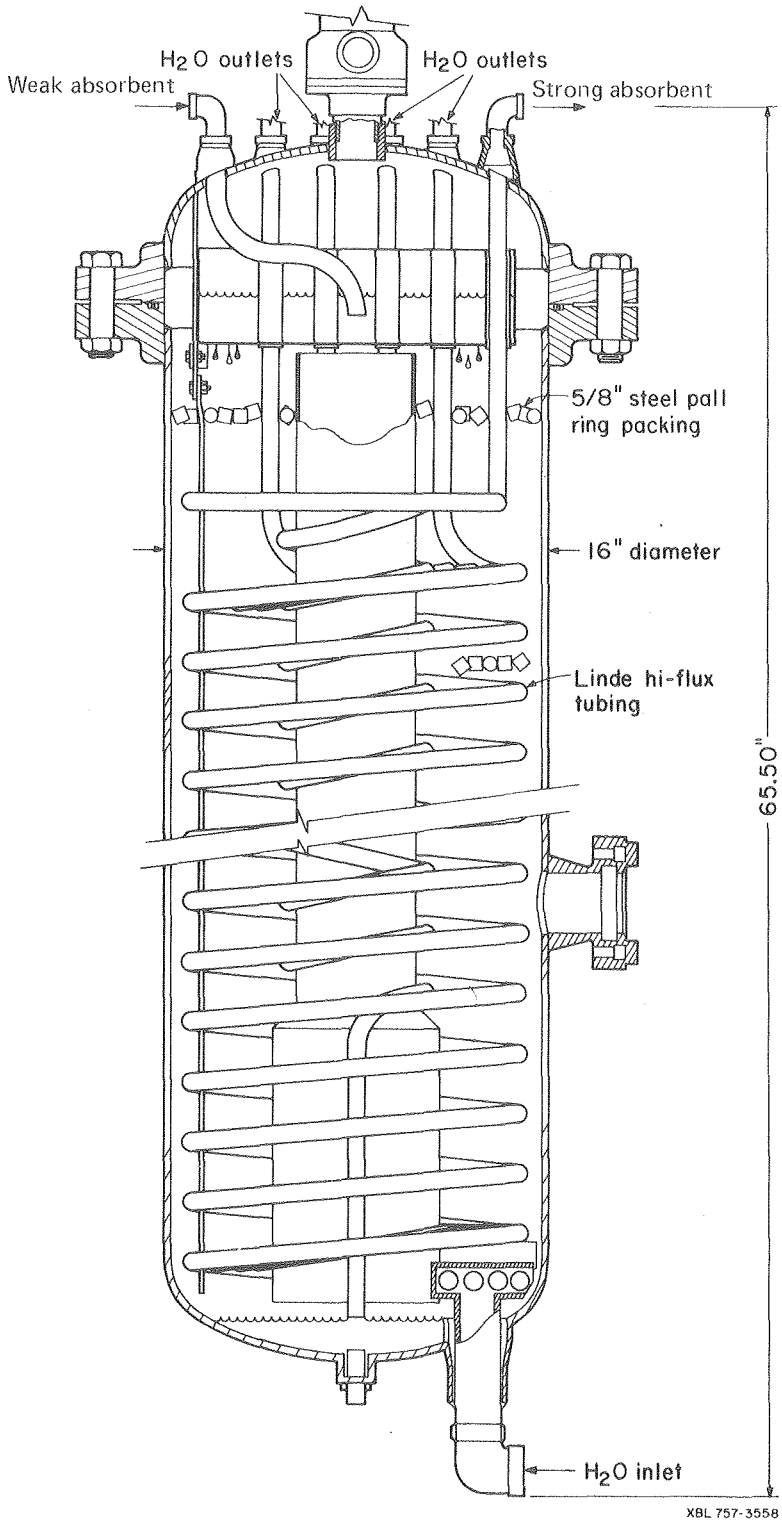

Fig. 15. The generator designed for operation with solar heated water. The Pall ring packing extends from the liquid distribution pan to the bottom layer of coils.

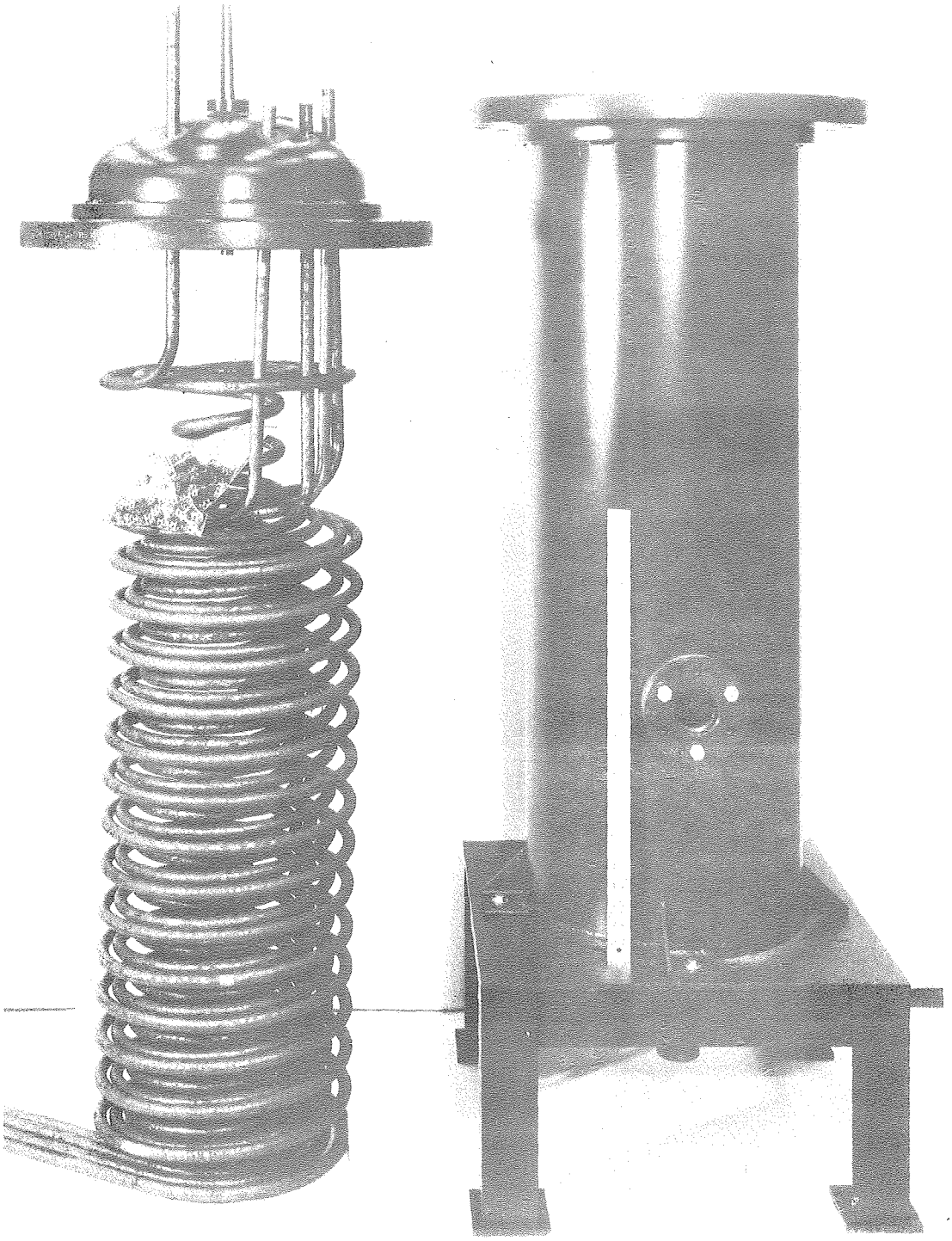

XBB 757-5474

Fig. 16. The coils wound from Linde Hi-Flux tubing and the generator shell.

APPENDIX II. EXPERIMENTAL DATA

Table 1. Pressure drop across the absorber.

Run number	ΔP_{total} † (psi)	ΔP for series coil ‡ (psi)	Ratio $\frac{m_{Vi}}{\dot{m}_{NH_3}}$ series coil	$\dot{m}_{WS}$ (lb/hr)	From evaporator $\dot{m}_{NH_3}$ (lb/hr)
1	3-1* = 2	3	0.45	211	16
2	4-1 = 3	3	0.53	310	19
3	4.5-1 = 3.5	4	0.59	328	30
4	10-1 = 9	8	0.60	537	30
5	9-1 = 8	8	0.56	413	41
6	7.5-1 = 6.5	5.5	0.50	345	39
7	11-1 = 10	9	0.58	438	35
8	9.5-1 = 8.5	8	0.53	390	47
9	9.5-1 = 8.5	8	0.52	341	51
10	6-1 = 5	5	0.46	207	52
10c	7-1 = 6	4	0.47	201	47.7

*It is necessary to subtract $P_{hydro} = 1$ psi from the ΔP_{total} because the two pressure gauges measuring ΔP_{total} are at different liquid levels. The 1 psi represents 2.5 ft of liquid. The error on the measurement of ΔP is ± 2 psi.

† $\Delta P_{total} = P_A - P_9 - P_{hydro}$

‡ $\Delta P_{\text{for series coil}} = P_8 - P_9 = \Delta P$ (See Fig. 2 for locations of P_A, P_8, and P_9.)

Table 2. Data for Figure 5, ΔP_S versus $(\dot{m}_L \cdot \dot{m}_V)^{0.9}$.

Run number	$\Delta P_S = \Delta P - \Delta P_{\ell.0}$* (psi)	$(\dot{m}_{Li} \cdot \dot{m}_{Vi})^{0.9}$ $(lbs/hr)^{1.8}$
1	3 - 0.18 = 2.8	755
2	3 - 0.35 = 2.6	1,435
3	4 - 0.39 = 3.6	2,540
4	8 - 1.00 = 7.0	3,958
5	8 - 0.64 = 7.4	3,964
6	5.5-0.47 = 5.0	2,928
7	9 - 0.71 = 8.3	3,710
8	8 - 0.59 = 7.4	4,088
9	8 - 0.48 = 7.5	3,880
10	5 - 0.21 = 4.8	2,352
10c	4 - 0.20 = 3.8	2,137

For series coil before reconnecting the absorber, where

$$\dot{m}_{Li} = \dot{m}_{WS} + \tfrac{1}{2}\,\dot{m}_{NH_3}$$

q11

$$\dot{m}_{Vi} = \left(\text{ratio}\,\frac{\dot{m}_{Vi,\text{series coil}}}{\dot{m}_{NH_3}}\right) \cdot \dot{m}_{NH_3}$$

*ΔP from Table 1.

$\Delta P_{\ell.0}$ is defined on page 16.

Table 3. Experimental data for pressure drop across the absorber (after reconnection).

Run number	ΔP_{total}*	$\dot{m}_{WS}$	$\dot{m}_{NH_3}$
11	3.5-1 = 2.5	600	40
12	5 - 1 = 4	620	35
13	4.5-1 = 3.5	555	28
15	4.0-1 = 3	600	23
16	3.5-1 = 2.5	574	27
17B	4 - 1 = 3	415	28
17C	3 - 1 = 2	412	42
17D	2.5-1 = 1.5	417	15
18	4.5-1 = 3.5	726	26
19A	5.5-1 = 4.5	719	24
19B	6 - 1 = 5	718	37
20A	6 - 1 = 5	731	42
20B	5 - 1 = 4	605	45
20C	4 - 1 = 3	410	46
21	4.5-1 = 3.5	445	46
22	6 - 1 = 5	564	71

*$\Delta P_{total} = P_A - P_9 - P_{hydro} = \Delta P$

(See Fig. 9 for locations of P_A and P_9)

Table 4. Data for Figure 6 ΔP_p versus $(\dot{m}_L \cdot \dot{m}_V)^{0.9}$

Run number	$\Delta P_p = \Delta P - \Delta P_{\ell.0}$ *	$(\dot{m}_L \cdot \dot{m}_V)^{0.9}$
11	2.5 - 0.21 = 2.3	8,754
12	4 - 0.23 = 3.8	7,995
13	3.5 - 0.19 = 3.3	5,920
15	3 - 0.21 = 2.8	5,320
16	2.5 - 0.20 = 2.3	5,905
17B	3 - 0.11 = 2.9	4,557
17C	2 - 0.11 = 1.9	6,521
17D	1.5 - 0.11 = 1.4	2,610
18	3.5 - 0.30 = 3.2	7,052
19A	4.5 - 0.30 = 4.2	6,505
19B	5 - 0.30 = 4.7	9,592
20A	5 - 0.30 = 4.7	10,926
20B	4 - 0.21 = 3.8	9,806
20C	3 - 0.11 = 2.9	7,047
21	3.5 - 0.12 = 3.4	7,586
22	5 - 0.19 = 4.8	13,877

*$\Delta P = \Delta P_{total}$ from Table 3.

Table 5. Generator performance data; experimental data for calculation of U.*

Run number	p_G (psia)	x_W	x_S	T'_{SS} (°F)	T_{15} (°F)	T_{16-17} (°C)	ΔT_{SS} (°F)	T_{SS} (°F)
22	235	0.484	0.542	168.6	159.7	5.8	0.1	168.7
21	240	0.478	0.562	165.0	150.5	6.8	-0.9	164.1
20A	211	0.489	0.520	166.5	153.5	3.5	-1.5	165.0
20B	212	0.490	0.525	165.5	154.3	3.3	-1.2	164.3
20C	209	0.486	0.538	160.8	153.2	4.7	0.0	160.8
19A	191	0.462	0.480	170.3	155.2	1.8	-2.5	167.8
19B	200	0.477	0.503	167.1	152.4	3.5	-1.8	165.3
18	197	0.479	0.497	167.6	154.9	1.6	-2.1	165.5
17B	185	0.466	0.500	162.2	150.6	3.9	-1.1	161.1
17C	191	0.477	0.526	157.2	148.2	4.7	-0.3	156.9
16	197	0.500	0.522	160.6	148.5	2.8	-1.5	159.1
15	211	0.498	0.517	167.1	154.2	2.9	-1.7	165.4
13	184	0.476	0.501	161.5	149.2	2.3	-1.8	159.7
11	194	0.427	0.461	177.0	172.4	2.9	0.1	177.1
10A	207	0.477	0.581	149.3	153.7	5.3	7.5	151.8
9	235	0.471	0.539	169.3	163.0	5.6	0.5	169.8
8	215	0.464	0.522	167.4	167.0	1.8	0.5	167.9
7	209	0.467	0.528	163.5	162.1	2.8	0.6	164.1
6	233	0.472	0.526	172.2	168.0	1.8	-0.3	171.9
5	227	0.470	0.531	169.0	162.0	5.5	0.4	169.4
4	209	0.480	0.525	164.2	162.5	2.2	0.4	164.6
3	235	0.496	0.542	168.6	169.7	1.0	0.6	169.2
2	214	0.477	0.508	171.1	171.0	0.4	0.1	171.2
1	203	0.471	0.509	166.5	162.5	1.3	-0.4	166.1

*See text from page 23, Section 3.5.

Table 6. Generator performance data; experimental data and U.

Run number	$T_{HW_{in}}$ (°F)	T_{16} (°F)	$T_{HW_{out}}$ (°F)	T_{SS} (°F)	Q_{HW} (Btu/hr)	ΔT_m (°F)	U (Btu/hr ft^2-F)	$\dot{m}_{WS}$ (lbs/hr)
22	198.7	185.0	177.1	168.7	49,600	10.83	127.2	564
21	200.5	188.4	182.6	164.1	49,900	15.1	92.0	411
20A	184.8	175.3	172.2	165.0	40,900	8.3	136.9	731
20B	184.5	175.5	173.3	164.3	36,100	9.0	111.4	605
20C	184.1	175.6	173.5	160.8	33,600	10.5	89.2	410
19A	185.7	175.8	172.4	167.8	34,600	6.9	139.0	719
19B	185.2	174.7	170.6	165.3	36,700	7.6	134.0	718
18	182.0	172.9	171.0	165.5	31,500	7.1	122.4	726
17B	181.2	172.2	168.4	161.1	27,300	8.1	93.4	415
17C	181.2	171.2	166.1	156.9	31,500	9.6	91.2	412
16	176.5	166.5	162.9	159.1	25,000	6.4	108.4	574
15	179.6	172.8	170.6	165.4	28,200	6.0	131.3	600
13	190.8	168.8	161.1	159.7	30,200	7.5	112.2	555
11	198.3	188.2	186.4	177.1	41,700	9.7	119.5	600
10A	190.2	177.3	174.7	151.8	31,900	17.4	50.9	207
9	199.2	188.6	186.4	169.8	35,000	13.4	72.7	341
8	196.7	184.5	180.9	167.9	38,100	12.6	84.0	390
7	191.7	181.8	178.9	164.1	43,000	12.2	98.0	418
6	199.4	187.9	188.2	171.9	32,500	13.8	65.6	345
5	196.9	186.6	185.5	169.4	41,200	13.0	88.1	402
4	189.1	177.4	175.6	164.6	46,400	11.3	113.6	517
3	191.7	181.6	182.7	169.2	27,900	11.7	66.1	328
2	189.7	180.0	183.0	171.2	21,200	10.7	55.0	310
1	188.6	177.8	181.4	166.1	22,500	12.9	48.4	209

Table 7. Generator performance results.

Run number	U (Btu/hr-ft^2-F)	$\dot{m}_{HW}$ (lbs/hr)	$\dot{m}_S = \frac{1}{2}(\dot{m}_{WS}+\dot{m}_{SS})$ (lbs/hr)	h_{SS} (Btu/hr-ft^2-F)	Log mean ΔTm (°F)	Log mean ($T_{wall}-T_{sol.}$) (°F)
22	127.2	2,300	600	151.5	10.8	9.1
21	92.0	2,790	451	103.4	15.1	13.4
20A	136.9	3,250	752	162.5	8.3	7.0
20B	111.4	3,210	628	127.8	9.0	7.8
20C	89.2	3,160	433	99.4	10.5	9.4
19A	139.0	2,600	731	167.4	6.9	5.7
19B	134.0	2,510	737	160.5	7.6	6.3
18	122.4	2,860	739	143.2	7.1	6.1
17B	93.4	2,135	429	106.2	8.1	7.1
17C	91.2	2,080	433	103.5	9.6	8.5
16	108.4	1,840	587	127.0	6.4	5.5
15	131.3	3,140	611	154.9	6.0	5.1
13	112.2	1,020	569	138.4	7.5	6.1
11	119.5	3,510	620	138.1	9.7	8.4
10A	50.9	2,060	233	54.5	17.4	16.2
9	72.7	2,740	366	79.7	13.4	12.2
8	84.0	2,380	413	93.9	12.6	11.3
7	98.0	3,360	445	110.3	12.2	10.8
6	65.6	2,900	364	71.1	13.8	12.7
5	88.1	3,620	428	97.8	13.0	11.7
4	113.6	3,440	542	130.4	11.3	9.8
3	66.1	3,070	343	71.6	11.7	10.8
2	55.0	3,120	319	58.8	10.7	10.0
1	48.4	3,120	218	51.3	12.9	12.2

Table 8. Experimental verification of equation (16).

Run number	Experimental					Calculated	
	e_{PH}	R + 1	Q_E Btu/hr	Q_G Btu/hr	COP	COP	Error (%)
22	0.854	8.9	31,400	49,600	0.633	0.663	-4.8
20A	0.798	16.4	21,100	40.930	0.516	0.553	-7.1
20B	0.813	14.5	21,100	36,070	0.585	0.578	+1.2
20C	0.860	9.8	22,650	33,580	0.674	0.657	+2.5
19A	0.766	30.8	12,980	34,640	0.375	0.384	-2.3
19B	0.786	20.2	18,450	36,680	0.503	0.497	+1.1
18	0.767	28.8	13,620	31,490	0.432	0.416	+3.7
17B	0.845	15.6	14,300	27,330	0.523	0.584	-11.7
17C	0.857	10.7	20,430	31,450	0.649	0.652	-0.4
16	0.815	22.4	13,140	24,960	0.526	0.535	-1.8
13	0.810	20.6	15,060	30,150	0.500	0.521	-4.2
10A	0.924	5.1	24,130	31,920	0.756	0.729	+3.5
9	0.906	7.8	24,560	35,010	0.702	0.680	+3.1
8	0.822	9.2	23,380	38,130	0.613	0.617	-0.6
6	0.863	9.8	19,262	33,150	0.593	0.620	-4.7

e_{PH} = effectiveness of the preheater

R = lbs of weak solution per lb of NH_3

Q_E = cooling load

Q_G = heat input to the generator

COP = coefficient of performance = Q_E/Q_G, calculated from simplified equation (16)

$$COP = \frac{580 - 0.72\ T_C - 0.23\ T_E}{580 + (T_G - T_A)\left[1.14(1 - e_{PH})(R + 1) + 0.8\right]}$$

Table 9. Experimental verification of equation (18).

Run number	Experimental							Calculated	
	T_C (°F)	T_A (°F)	T_G (°F)	ΔP (psi)	a (psi)	Δx	T_E (°F)	T_E (°F)	Error (°F)
22	107.0	111.4	185.0	11.0	390	0.058	60.1	61.2	-1.1
20A	99.5	106.0	175.3	13.5	360	0.031	53.4	54.4	-1.0
20B	100.0	105.2	175.5	10.5	360	0.035	52.3	53.4	-1.1
20C	99.0	101.3	175.6	6.8	340	0.052	48.1	50.5	-2.4
19A	93.5	94.3	175.8	11.0	290	0.018	37.9	35.6	+2.3
19B	96.0	100.4	174.7	12.5	320	0.026	45.2	46.3	-1.1
18	95.5	99.0	172.9	11.0	320	0.018	44.6	43.5	+1.1
17B	91.5	91.8	172.2	6.4	280	0.034	34.5	35.2	-0.7
17C	93.5	95.9	171.2	6.0	310	0.049	43.0	43.1	-0.1
16	95.5	102.6	166.5	8.5	360	0.022	48.7	51.6	-2.9
13	91.0	94.6	168.8	8.0	300	0.025	39.4	39.0	+0.4
10A	98.5	95.4	177.3	8.0	320	0.104	51.8	52.1	-0.3
9	107.0	101.8	188.6	11.5	340	0.068	50.9	53.0	-2.1
8	100.7	100.0	184.5	13.0	340	0.058	51.3	48.2	+3.1
6	106.3	96.0	187.9	11.0	320	0.054	46.8	44.6	+2.2

T_C = condensing temperature

T_A = absorbing temperature

T_G = generating temperature

ΔP = pressure drop across the absorber

a = $(\partial P/\partial x)_{T_A}$, saturated solution, evaluated at mean concentration

T_E = evaporating temperature, calculated from:

$$T_E = 3.2 + 1.82(T_C + T_A)/2 - 0.852\ T_G + (1.07 - 0.0097\ T_E)(\Delta p + a\Delta x)$$

Δx = concentration difference between the strong and the weak solutions

This report was done with support from the United States Energy Research and Development Administration. Any conclusions or opinions expressed in this report represent solely those of the author(s) and not necessarily those of The Regents of the University of California, the Lawrence Berkeley Laboratory or the United States Energy Research and Development Administration.

0 0 0 0 4 5 0 2 2 9 4